ACS APPLIED MATERIALS & INTERFACES

www.acsami.org

Research Article

Sequential and Switchable Patterning for Studying Cellular Processes under Spatiotemporal Control

Themistoklis Zisis,[#] Jan Schwarz,[#] Miriam Balles, Maibritt Kretschmer, Maria Nemethova, Remy Chait, Robert Hauschild, Janina Lange, Calin Guet, Michael Sixt,* and Stefan Zahler*

Cite This: *ACS Appl. Mater. Interfaces* 2021, 13, 35545−35560

Read Online

ACCESS | Metrics & More | Article Recommendations | Supporting Information

ABSTRACT: Attachment of adhesive molecules on cell culture surfaces to restrict cell adhesion to defined areas and shapes has been vital for the progress of in vitro research. In currently existing patterning methods, a combination of pattern properties such as stability, precision, specificity, high-throughput outcome, and spatiotemporal control is highly desirable but challenging to achieve. Here, we introduce a versatile and high-throughput covalent photoimmobilization technique, comprising a light-dose-dependent patterning step and a subsequent functionalization of the pattern via click chemistry. This two-step process is feasible on arbitrary surfaces and allows for generation of sustainable patterns and gradients. The method is validated in different biological systems by patterning adhesive ligands on cell-repellent surfaces, thereby constraining the growth and migration of cells to the designated areas. We then implement a sequential photopatterning approach by adding a second switchable patterning step, allowing for spatiotemporal control over two distinct surface patterns. As a proof of concept, we reconstruct the dynamics of the tip/stalk cell switch during angiogenesis. Our results show that the spatiotemporal control provided by our "sequential photopatterning" system is essential for mimicking dynamic biological processes and that our innovative approach has great potential for further applications in cell science.

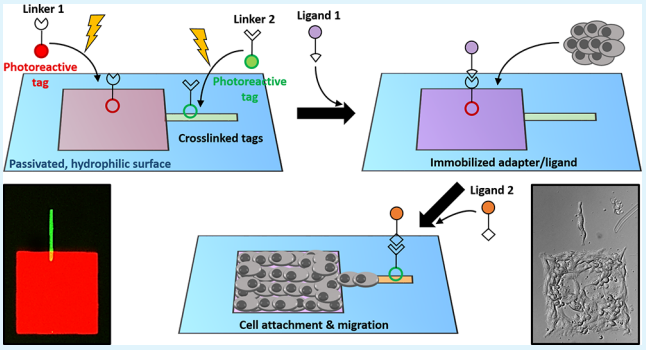

KEYWORDS: *surface engineering, photopatterning, click chemistry, microcontact printing, integrin*

INTRODUCTION

Spatially controlled deposition of extracellular signaling or adhesion molecules on cell culture surfaces (also described as micropatterning) became an essential tool in all experimental fields operating with cultured cells.[1−6] "Printing" molecules on surfaces to acquire spatial control over cell microenvironments is essential for understanding processes such as cell division, differentiation, adhesion,[7−9] and migration,[10,11] which are highly dynamic.

The key challenges in such surface engineering are stability, precision, and specificity. This does demand not only minimal background deposition of the applied biomolecule but ideally also avoidance of binding of unspecific bystander molecules (like serum factors). This is usually achieved by employing inert (passivated) background chemistry. Precision demands the option to immobilize quantitatively and ideally with submicron resolution. This includes not only digital patterns with submicron resolution but also the generation of continuous gradients.[12,13] Furthermore, surface immobilization is preferably based on covalent modifications so that deposition is stable and sustainable, thereby permitting long-term applications, e.g., well-free cell culture systems.

Using structured illumination for patterning not only provides a method to covalently bind adhesive peptides or other molecules but also enables high-throughput fabrication approaches, such as creating small adhesion spots for single-cell screenings over large cell culture surfaces.

Microcontact printing[14] has provided a spatiotemporally controllable setup for understanding cell mechanosensing.[15−17] However, a significant disadvantage of the conventional microcontact printing techniques is the variability in the quality of protein transfer and requirement of bulky macromolecules (i.e., extracellular matrix or ECM proteins) to create the desired patterns. This limits the applicability of such methods to settings where one or more different biomolecules are added in the process, as unwanted nonspecific interactions can take place, influencing the experimental outcome. Moreover, the stability of proteins can be significantly reduced

Received: May 28, 2021
Accepted: June 29, 2021
Published: July 20, 2021

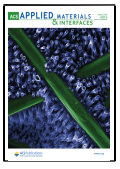

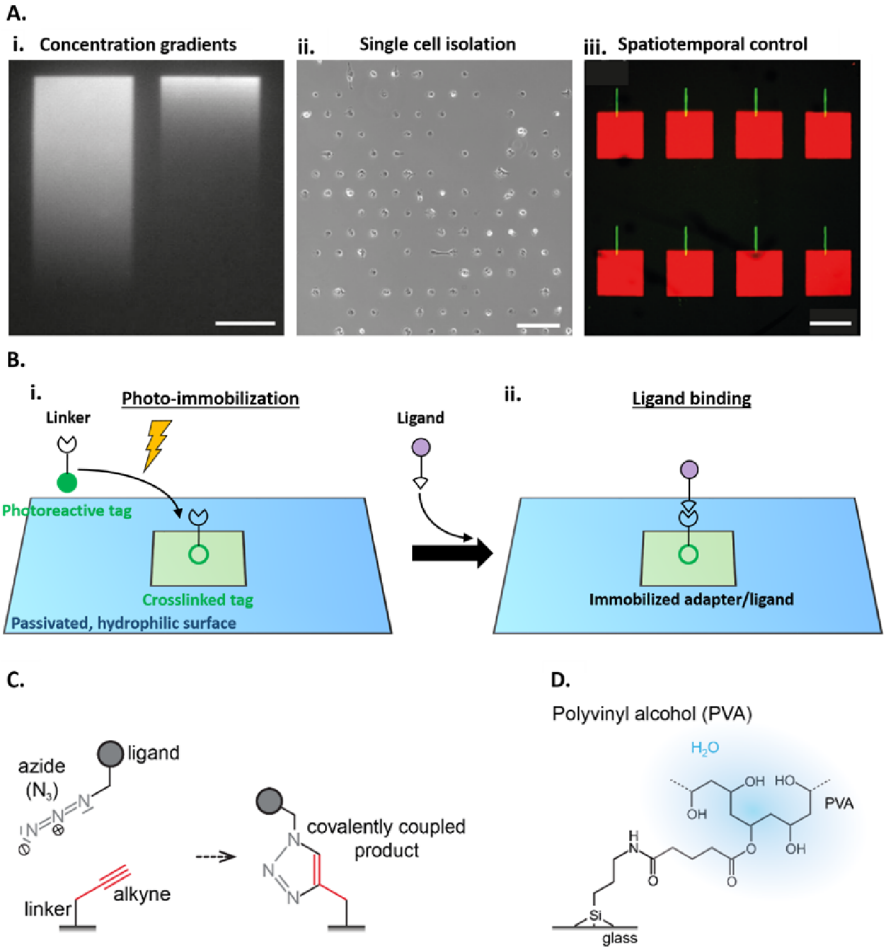

Figure 1. Covalent protein patterning by photobleaching. (A) Application examples for 2D surface modification by micropatterning. (i) Control on adhesion influenced haptotactic cell migration on gradients of adhesion cues. Scale bar: 100 μm. (ii) Control on the cell number, shape, and density by single-cell adhesion grids. Scale bar: 200 μm. (iii) Spatiotemporal control of cell migration by two-step surface adhesion. Scale bar: 250 μm. (B) Schematic of building-block-based photopatterning. (i) Surface immobilization of photo-cross-linker-labeled linker molecules by photo-immobilization. (ii) Immobilization of ligands via the adapter system. (C) Cu(I)-catalyzed 1,3 dipolar cycloaddition as an adapter system of soluble, ligand-bearing azides (N3) and photoimmobilized alkynes for covalent ligand binding. A small, ~70 Da, triazole adapter is present between the surface and immobilized dye. (D) Passivating hydrogel layer (polyvinyl alcohol (PVA)). The PVA polymer covalently binds to the amino-silanized glass surface, forming a hydrated passivating layer.

Table 1. Photoreactive Subunits

	AbsMAX	kinetics	autofluorescence	commercial availability
		Fluorescent Dye		
for example, 6-FAM	470 nm	slow	yes, full spectrum	yes
		Norrish Type II Photoinitiators		
for example, 4-benzoylbenzoic acid based	~300 nm	slow	yes, blue spectrum	yes
diazirine based	~360 nm	fast	no	used in commercial cross-linkers[25]

over time, making the whole setup time sensitive. Here, we introduce a covalent, building-block-based, versatile photo-immobilization technique. It comprises a light-dose-dependent patterning step, which is feasible on arbitrary surfaces, enabling the production of sustainable patterns and gradients. We validate the method by photopatterning of adhesive ligands on cell-repellent surface coatings, thereby confining cell growth and migration to the designated areas and gradients. In the second step, we added a further layer of complexity by enabling spatiotemporal control over two distinct light-switchable surface patterns. This gives unprecedented access to studying time-dependent cellular processes in vitro.

RESULTS AND DISCUSSION

Overview of the Building-Block-Based Photopatterning Technique and Its Components. Building-block-based patterning can be used for 2D surface modification in various applications, from generation of adhesion cue gradients to single-cell adhesion grids and spatiotemporally controlled cell adhesion patterns (Figure 1A(i–iii)). This photopatterning technique combines two orthogonal reaction steps to surface immobilize molecules in a bioactive monolayer. In the first step, a linker molecule labeled with a photoreactive tag and an adapter group is covalently immobilized on any surface by structured illumination (Figure 1B(i)).[18,19] In the second step,

https://doi.org/10.1021/acsami.1c09850
ACS Appl. Mater. Interfaces 2021, 13, 35545−35560

Table 2. Adapter Chemistry

cross-linker	ligand	catalyst necessary	catalyst	side reactions
terminal alkyne	azides	yes	Na-ascorbate, $CuSO_4$, and BTTAA	orthogonal in physiological milieu
		Strained Alkyne		
DBCO	azides	no		orthogonal in physiological milieu
BCN	azides	no		orthogonal in physiological milieu
terminal azide	alkynes (strained and terminal)	depending on alkynes used; see above		orthogonal in physiological milieu

Table 3. Adhesion Ligands

	matrix protein	sequence	fluorescence	commercial availability
GRGDS[a]	fibronectin	integrin-binding sequence	no	yes
Hilyte555-GRGDS	fibronectin	integrin-binding sequence; dye coupled	λ_{MAX} 566 nm	no
cRGD[b]	fibronectin	cyclic integrin-binding sequence	no	yes

[a]Glycine−arginine−glycine−aspartic acid−serine. [b]Cyclic arginine−glycine−aspartic acid.

the relevant ligand for the desired biological setup is covalently attached to the surface-bound linker via an adaptor system (Figure 1B(ii)). Separation of the photoimmobilization and the ligand-binding step hereby prevents degradation of the ligand during illumination. Thus, only active and accessible ligands are presented on the surface. An established patterning process can easily be adapted to another biological system, making the building-block-based photopatterning method very versatile. We test several photoreactive molecules, adapter systems, cell-adhesive ligands, surface passivation agents, and illumination methods for building-block-based photopatterning. Different combinations of the aforementioned components are implemented for different biological applications, and their compatibility and efficacy are discussed.

Photoreactive Molecules. Photoreactive subunits can be selected from a plethora of photoreactive molecules (Table 1), which, in their activated state, form highly reactive intermediates, such as radicals, carbenes, and nitrenes. Fluorescent dyes represent a very easily accessible class of photoreactive molecules. Activated at their specific absorption maximum, fluorescent dyes can fragment and form unspecific and often long-lived radicals,[18] which in turn are able to react with many surfaces. This "photobleaching" process leads to an effective immobilization of the fluorescently tagged linker. Bleaching-prone dyes, such as 6-FAM, thereby bind with higher efficiency than modern bleaching-resistant ones.[20] Due to slow kinetics and the possibility of unspecific dye fragmentation and multimerization, fluorescent dyes are prone to produce high unspecific background binding and are often excitable by the full fluorescence spectrum, leading to detectable background autofluorescence after immobilization.

Norrish Type II photoinitiators, such as 4-benzoylbenzoic acid, are widely used as photo-cross-linking molecules[21,22] due to their cross-linking capabilities and fast reaction kinetics. However, with absorption maxima around 300 nm, activation necessitates light sources with high intensities in the UV-B range and therefore special optics and filters. Additionally, solubility in aqueous solution is rather poor, limiting the available working concentrations. Diazirine-based photoreactive molecules can be activated at wavelengths in the UV-A range and show fast reaction kinetics and no autofluorescence after the reaction. Due to their small size, solubility of the linker molecule in aqueous solution is not hampered by the addition of a diazirine.[23−25]

Click Chemistry of the Adaptor System Adapter. Due to their covalent character, versatility, and specificity, we chose 3 + 2 cycloadditions such as the alkyne/azide "click" system serving as a chemical adapter system to connect a surface-immobilized linker with a biologically relevant ligand (Figure 1C and Table 2).[26] Here, azide-conjugated molecules or proteins are covalently attached to photoimmobilized alkynes or vice versa. Azide- or alkyne-modified dyes, amino acids, proteins, and nucleic acids as well as labeling reagents and kits are commercially available and inexpensive due to the rising importance of click-chemistry-related techniques. Using strain-aided cycloaddition reactions,[27] reactions can be carried out without the use of catalysts such as copper(I) salts. Replacing the terminal alkyne by BCN (bicyclo[6.1.0]nonyne), for example, allows the ligand immobilization in cell culture medium under physiological conditions. Therefore, through sequential photopatterning, two-step adhesion experiments, where certain areas are functionalized with the binding motif in the presence of cells, are possible.

Ligand. In contrast to microcontact printing, photopatterning does not necessarily require the use of bulky proteins for cell adhesion, although it is still an option,[21,22,28] but can implement adhesive components such as small binding motifs (SBMs).[29] SBMs are short amino acid sequences of large ECM proteins, which are high-affinity integrin ligands and therefore cell adhesive. One of the most commonly used SBMs is the RGD (arginine−glycine−aspartic acid) motif, found in many well-characterized ECM proteins like fibronectin or collagen. RGD peptides or similar SBMs are often preferred over complete ECM proteins, in regard to cell adhesion, due to their higher solubility and lower sensitivity to denaturation.[30−32] However, not all integrins are adhesive to RGDs, including laminin-binding, collagen-binding, and leukocyte integrins.[33] Furthermore, RGD-binding integrin subtypes exhibit different affinities for RGDs. For example, integrins $\alpha v\beta 3$ and $\alpha 5\beta 1$ are high-affinity RGD targets, while $\alpha v\beta 6$, $\alpha v\beta 8$, and $\alpha IIb\beta 3$ integrins show lower binding to RGDs.[34,35] Moreover, integrin expression is highly variable according to the cell and tissue type, for example, platelets primarily express $\alpha IIb\beta 3$ integrins or leukocytes express leukocyte integrins and are therefore less likely to bind to RGDs.[35] In this study, we test cells with high RGD affinity such as 3T3 fibroblasts, zebrafish keratocytes, and renal cell carcinoma (RCC) cells that adhere to our RGD-coated surface very efficiently. We also use human microvascular endothelial

https://doi.org/10.1021/acsami.1c09850
ACS Appl. Mater. Interfaces 2021, 13, 35545−35560

cells (HMECs), which exhibit lower RGD affinity, but increasing the RGD density on the surface significantly improves attachment. Furthermore, for cell types expressing integrins that are not adhesive to RGDs, there are multiple other ligand options, i.e., GFOGER sequence from collagen 1[36] and A5G81 and YGISR sequences from laminin,[37] which are still compatible with this photopatterning process. Thus, the applicability of this method is not limited to the cell lines tested here or to cell lines highly adhesive to RGDs but can incorporate a wide variety of cell types.

In this study, we chose different commercially available RGD versions to induce cell adhesion on passivated, cell-repellent surfaces (Table 3). Linear RGD sequences, such as the GRGDS (glycine−arginine−glycine−aspartic acid−serine) motif, are commercially available and can easily be fluorescently tagged (Hilyte555-GRGDS). The integrin activation capability, however, was shown to be increased if not only the motif sequence but also the motif structure of the native ECM protein is mimicked.[32,38] Therefore, a cyclic RGD motif variant (cRGD) was used as well.

Passivation. Especially for surface immobilization of adhesive ligands, covalent attachment is crucial to enable proper force transduction of the cells onto the substrate. Similarly, sustainable passivation is necessary to avoid uncontrolled background adhesiveness. For surface passivation, highly hydrophilic and passivating polyol-based hydrogels, which can be bound covalently to the underlying surface, are favored. Thin polyol films are offering excellent antiadhesive properties over long time periods and, in contrast to passivating monolayers, such as PEG-based self-assembled monolayers or block polymers,[39−41] can be efficiently modified by photobleaching.[42,43] Furthermore, polyol films do not alter imaging properties of the underlying imaging bottom. In this study, we use commercially available polyol-coated 8 Well and channel slides (μ-Slide VI$^{0.4}$ Bioinert and μ-Slide 8 Well^{high} Bioinert, ibidi GmbH) and PVA-coated aminosilanized glass coverslips (Figure 1D)[44] as a cell-repellent base material.

Illumination. To create 2D patterns, the photoreactive cross-linker needs to be illuminated and therefore excited locally on the passivated surface. Illumination can be carried out by different devices depending on the application, technical adaptivity, resolution, and throughput requirements (Table 4).

Table 4. Illumination Devices

collimated LED (photomask based)	scanning laser	LCD projector
collimated lens	advanced optics	advanced optics
any light source possible	laser	any light source
cheap and simple setup	expensive setup	expensive setup
high throughput	low throughput	low throughput
fast	slow	slow
low resolution	high resolution	medium resolution
no intensity gradient possible	intensity gradient possible	intensity gradient possible

While microscope-based illumination allows for high resolution due to the microscope optics, collimated light sources like LEDs can illuminate large areas and therefore allow for high-throughput illumination. For structuring the illumination, microscope-based approaches use scanning lasers or spatial light modulators (SLMs, e.g., LCD projectors). Both allow for gradual tuning of illumination intensities, which result in immobilized ligand concentration gradients.

The power of the presented building-block-based micropatterning approach is the versatility regarding applications and substrates. In the following sections, different combinations of photoreactive linkers, coupling chemistry, and illumination setups are used to create micropatterns for very specific applications.

Development and Assessment of Single Photopatterning Technique Using Different Cell Lines. *Generation of Concentration Gradients to Study Haptotactic Cell Migration.* Haptotactic cell migration is a crucial biological process, for example, in immunology and development.[11,45,46] Cellular mechanisms underlying haptotactic cell migration are still not fully understood. To understand these mechanisms, we sought to create concentration gradients of cell-adhesive ECM ligands offering defined shapes and local concentrations. As a passivated, cell-repellent surface, we coated glass coverslips with a thin layer of PVA hydrogel.[43] 6-FAM-alkyne was used as a photo-cross-linker, which was immobilized on the PVA-coated glass via structured illumination (Figure S1A). Patterns and gradients were generated by a 470 nm LED light source and a controllable LCD panel of a commercially available projector inserted into the light path of an epi-fluorescence microscope.[47] The photo-cross-linker 6-FAM-alkyne with its absorption maximum at ∼470 nm allowed us to use blue light instead of UV light for photopatterning. Thus, expensive UV light-compatible SLMs and optics could be avoided. To visualize and quantify the generated pattern and gradients during the experiment, azide-conjugated linear fibronectin-SBM-GRGDS carrying a fluorescent tag (HilyteFluor555) was used as a cell adhesion ligand (Figure S1A,B).

In the first step, we tested different illumination times and analyzed the amount of surface-bound SBM. Increasing the duration of illumination at maximal power showed a surface saturation of 6-FAM-alkyne at high illumination times and subsequently GRGDS-HilyteFluor555 (referred to as RGD-HF-555 for simplicity) and a simultaneous increase in background fluorescence. This results in an optimal illumination time of 10 min where the contrast between the fluorescence signal in the illuminated regions and the background is at its maximum (Figure S1C). With this setup, a maximal concentration of 653 ± 24 molecules/μm^2 could be achieved at 10 min of illumination (Figure S1D).

Next, we tested the bioactivity of immobilized RGD-HF555 and the effectivity of the cell-repellent PVA coating. Therefore, we printed RGD-HF555 patches offering ideal adhesiveness for migrating zebrafish keratocytes and adhesive growing 3T3 mouse embryonic fibroblasts (3T3 fibroblasts) (Figure 2A). Zebrafish keratocytes and 3T3 fibroblasts only adhered in the RGD-HF555-patterned areas (100% relative light intensity). Adhesion in nonpatterned areas (0% relative light intensity) was only rarely observed (Figure 2B). Similar to adhesion, zebrafish keratocyte migration was confined to RGD-HF555-patterned regions, as illustrated by cell trajectories (Figure 2C). Although highly motile, the cells were not able to cross the RGD-HF555/PVA interface and were forced to repolarize and change the direction (Movie SM1). 3T3 fibroblast growth within the patterned regions was stable also in long-term cultures grown beyond confluency (Figure 2C). This verifies the long-term stability of the covalent PVA surface passivation and, accordingly, the RGD-HF555 immobilization on PVA, making this setup suitable for long-term experiments.

Fish keratocytes show an oval, fan-shaped morphology when migrating. To influence their cell spreading and eccentricity,

https://doi.org/10.1021/acsami.1c09850
ACS Appl. Mater. Interfaces 2021, 13, 35545−35560

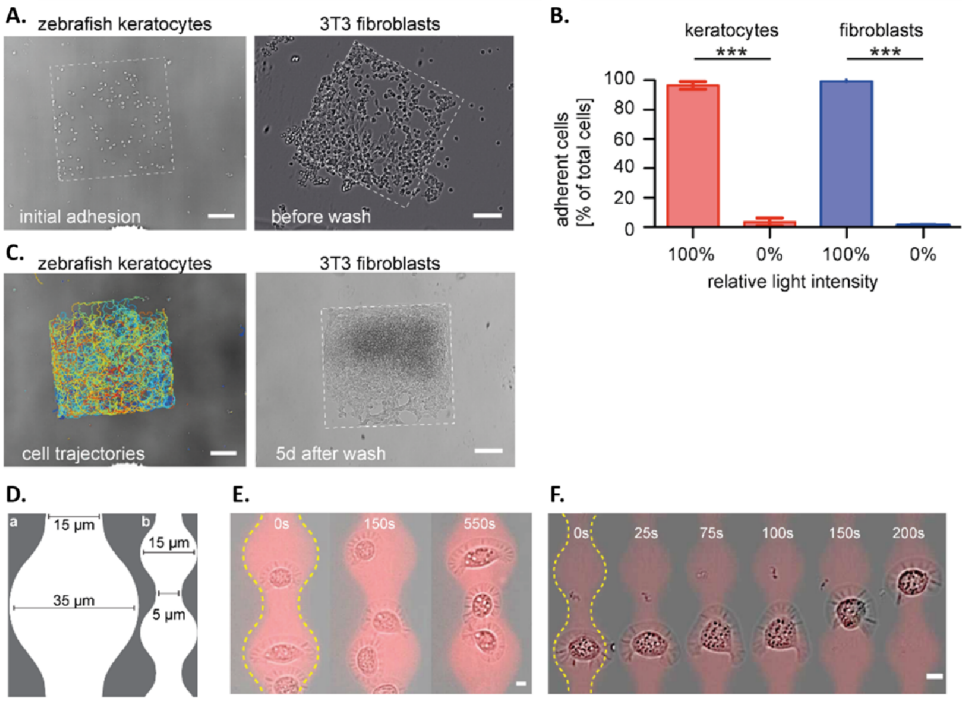

Figure 2. Characterization of RGD-HF555 photopatterning on passivating PVA coating as a tool for probing cell migration. (A) Bright-field images of zebrafish keratocytes and 3T3 fibroblasts (t = 3 h after seeding (before wash)) adhering and growing on square patches of RGD-HF555. Scale bar: 100 μm. (B) Fraction of zebrafish keratocytes (red bars, $p < 0.0001$) or 3T3 fibroblasts (blue bars, $p < 0.0001$) adhering on (100% intensity) or next to (0% intensity) 450 × 450 μm^2 square patches of RGD-HF555. (C) Zebrafish keratocytes migrating on a patch of RGD-HF555 printed on the PVA background. Cell trajectories after t = 2 h. Scale bar: 100 μm. (D) Bright-field image of 3T3 fibroblasts on square patches of RGD-HF555 grown for 5 days. Scale bar: 100 μm. (E) Template for alternating wide and narrow adhesive areas influencing cell shape changes during migration. (F) Zebrafish keratocyte migrating on 35-μm-wide areas of RGD-HF555 with 15 μm constrictions. Scale bar: 5 μm. (G) Zebrafish keratocyte migrating on 15-μm-wide areas of RGD-HF555 with 5 μm constrictions. Scale bar: 5 μm.

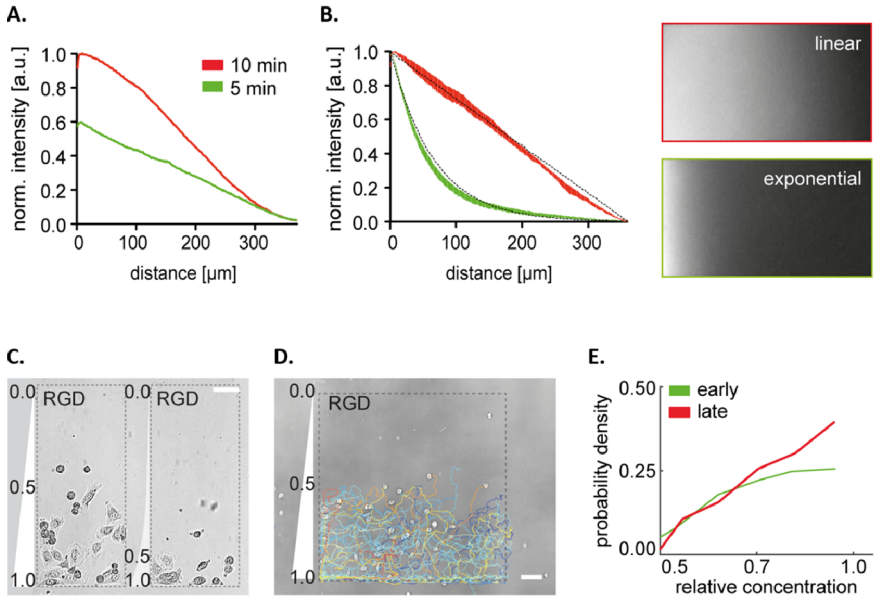

Figure 3. Photopatterning of concentration gradients of surface-immobilized RGD-HF555 on passivating PVA coating as a tool for probing haptotactic cell migration. (A) Normalized intensity profiles of linear gradients of RGD-HF555. Gradient steepness dependent on the 470 nm LED exposure time. Green profile: 5 min exposure time. Red profile: 10 min exposure time. (B) Normalized intensity profiles of linear and exponential-like gradients of RGD-HF555. Green profile: 5 min exposure time and exponential mask. Red profile: 5 min exposure time and linear mask. In (C)−(E), relative RGD-HF555 concentration is given as relative light intensity. (C) Bright-field image of 3T3 fibroblasts adhering and migrating on linear (left) and exponential (right) gradients of RGD-HF555. Scale bar: 50 μm. (D) Bright-field image of zebrafish keratocytes migrating on a linear gradient of RGD-HF555. Scale bar: 50 μm. (E) Time-dependent zebrafish keratocyte trajectory distribution within a linear gradient of RGD-HF555. Early: t = 0−60 min and late: t = 61−120 min (n = 5 independent experiments).

https://doi.org/10.1021/acsami.1c09850
ACS Appl. Mater. Interfaces 2021, 13, 35545−35560

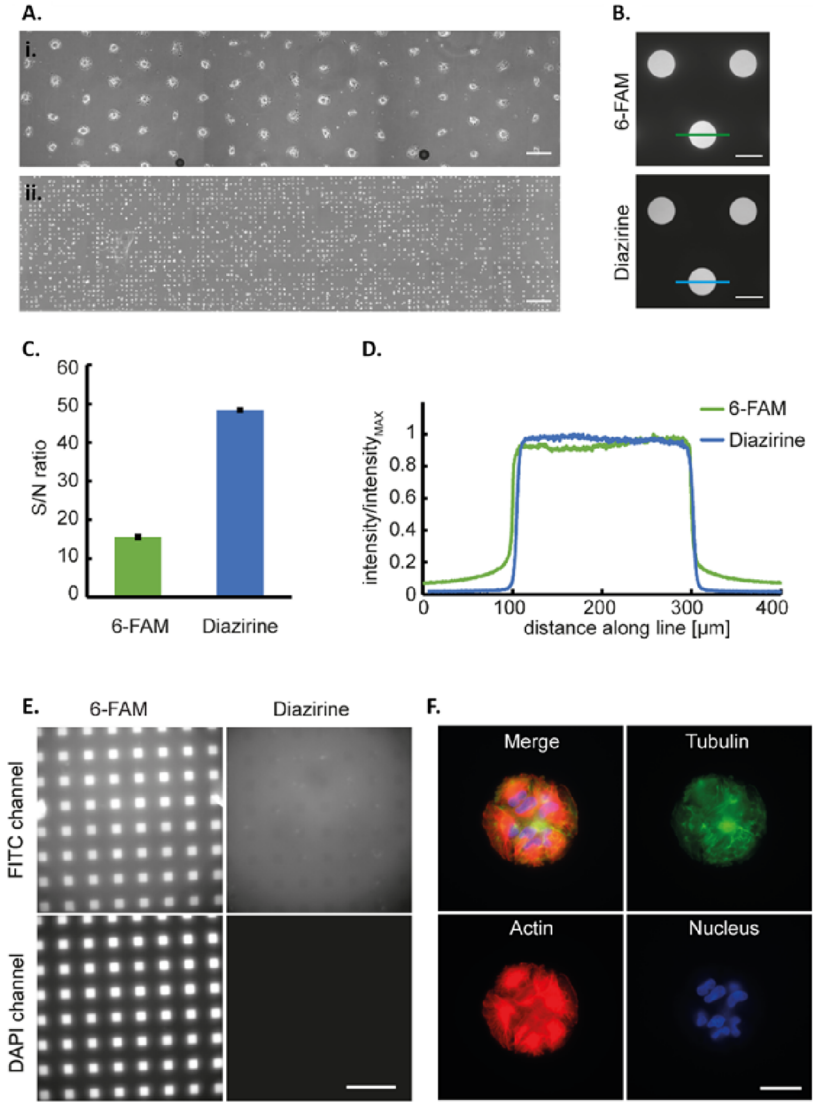

Figure 4. Use of a diazirine linker to generate large patterned areas with very low background immobilization and advanced fluorescence properties. (A) Cells ((i) RCC and (ii) NIH 3T3)) seeded in a microchannel of an ibidi μ-Slide VI$^{0.4}$ Bioinert where the whole channel is patterned with adhesion spots of (i) 200 μm and (ii) 35 μm diameter using a collimated LED and a photomask. Images were taken (i) 3 days and (ii) 4 h after seeding. Scale bar: 400 μm. (B) Fluorescence images of sulfo-Cy3-azide coupled to either a photopatterned 6-FAM-alkyne or a diazirine-alkyne spot. Green and blue lines indicate the position of the fluorescence intensity profile from (D). Scale bar: 200 μm. (C) Signal-to-noise ratio of the 200 μm pattern generated either with 6-FAM-alkyne or diazirine-alkyne and visualized by functionalizing the pattern with a sulfo-Cy3-azide. (D) Sulfo-Cy3-azide intensity profile across a 200 μm wide pattern spot generated by structured illumination of either 6-FAM-alkyne or diazirine-alkyne (profile along the green/blue line shown in Figure 3B). (E) Autofluorescence in the FITC or DAPI channel of the pattern of 30 μm wide squares generated by either structured illumination of 6-FAM-alkyne or diazirine-alkyne. Scale bar: 200 μm. (F) Immunofluorescence staining of RCC cells on the 100 μm circular pattern: green phalloidin staining, red tubulin staining, and blue DAPI staining. Scale bar: 50 μm.

the available adhesion area can be changed. To illustrate this, we spatially confined migration of fish keratocytes in alternating wide and narrow regions of RGD-HF555 (Figure 2D−F). In 35 μm wide areas, cells showed a fanlike lamellipodium that collapsed in narrow 15 μm wide constrictions (Figure 2E and Movie SM2). In 15 μm wide areas with 5 μm constrictions (corresponding to half a cell diameter), parts of the lamellipodium protruded along the constriction, trailing the bigger cell body to the next wide area (Figure 2F and Movie SM3). For both geometries, cells moved only on patterned areas, avoiding passivated background areas.

By using an SLM-modified microscope as an illumination system, gradients of different shapes and intensities can easily be patterned. The precise control of concentration gradient properties, such as shape and steepness of signaling or adhesive cue gradients, is essential for understanding processes like haptotaxis.[10,48] To illustrate the ability to generate arbitrary homogeneous gradients, we patterned concentration gradients of RGD-HF555 differing in maximal concentration and steepness by changing the illumination time (Figure 3A). The ability to create gradients of different shapes is illustrated by patterning squares with linearly and exponentially decreasing concentrations of surface-bound RGD-HF555 (Figure 3B). This is a big advantage of the presented photopatterning approach as forming such gradients within a protein coating setup is very demanding and hard to achieve.

3T3 fibroblasts adhering to linear and exponential RGD-HF555 gradients migrated and grew in a polarized manner in

https://doi.org/10.1021/acsami.1c09850
ACS Appl. Mater. Interfaces 2021, 13, 35545−35560

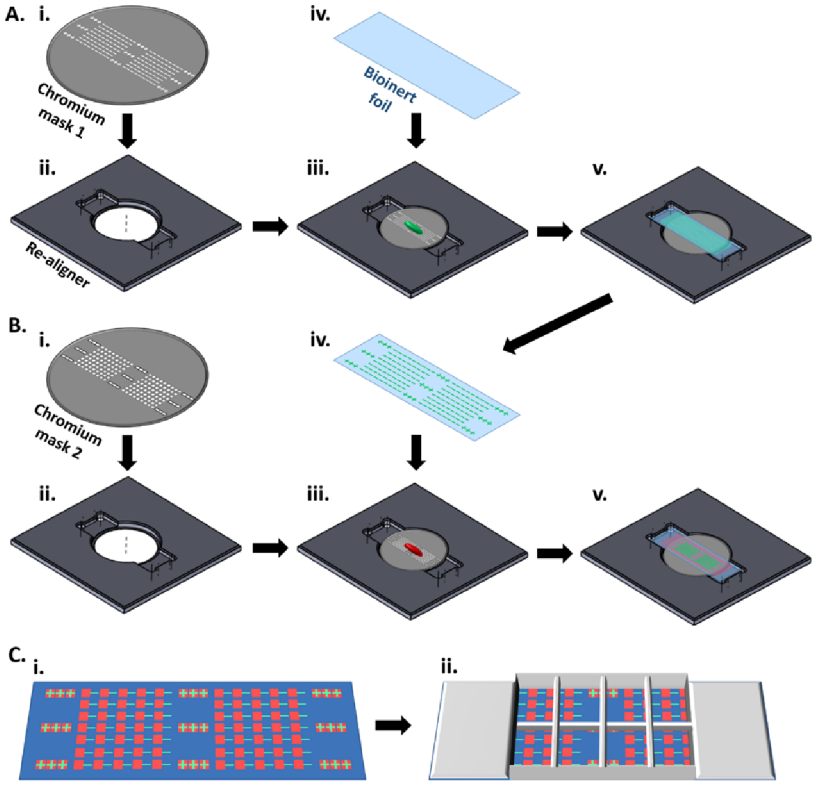

Figure 5. Schematic illustration of the sequential photopatterning process of the "dynamic" system. (A) Photopatterning of the tip area. (i) Chromium mask etched in a line patterned manner, with cross-shaped alignment markers on either side of the main patterns. (ii) Custom-made realigner designed to coordinate the two masks. (iii) Added dye linker (6-FAM-azide) solution, here shown in green and (iv) ibidi's Bioinert foil. (v) Configuration of first mask-dye-foil, illuminated from underneath, producing the desired pattern on the foil. (B) Photopatterning of the stalk area. (i) Second chromium mask etched in a square-patterned manner, with square-shaped alignment markers on either side of the main patterns. (ii) Custom-made realigner coordinating the two masks. (iii) Second added dye linker (diazirine-alkyne) solution, here shown in red. (iv) Line-patterned foil resulting from illumination through the first mask. (v) Final configuration of second mask-dye-foil, illuminated from underneath. Crossover square alignment markers were used to precisely align the foil's existing pattern with the pattern of the second mask. (C) (i) Resulting final line (tip) and square (stalk) photopatterned surface on the Bioinert foil, shown in green and red, respectively. Crossover square alignment markers shown on either side of the mail patterns. (ii) Attachment of an adhesive 8-well bottomless μ-Slide on the patterned surface of the foil, enabling later addition of click reaction solutions and cell seeding.

the direction of maximal RGD concentration (Figure 3C and Movie SM4). Similarly, highly motile zebrafish keratocytes migrated preferentially in areas of a linear RGD-HF555 gradient where adhesiveness was highest for the assayed concentration range (Figure 3D and Movie SM5). Hereby, cell trajectories shifted to highest RGD-HF555 concentrations over time (Figure 3E), demonstrating haptotactic behavior of zebrafish keratocytes on gradients of RGD-HF555.

Use of Collimated LEDs for High-Throughput Photopatterning. Microscope objective-based illumination systems like the one used above are flexible but rely on sequential illumination, thereby limiting the throughput in generating photopatterns. In biological and pharmaceutical applications, including screenings on 3D cell cultures or single cells, multiple parallel measurements are often desirable.[49−52] For these applications, large areas need to be structured in a short time period. For such a purpose, we devised a simplified structured illumination setup, consisting only of a collimated LED light source and a photomask (Figure S2A). Here, a whole microslide or even microplate can be illuminated simultaneously. The optics of the SLM/microscopy setup are also not compatible with UV excitable photoinitiators. Instead, collimated LEDs with emission at 360 nm are commercially available for very low prices. Thereby, the use of collimated LEDs allows the implementation of nonfluorescent photo-cross-linking subunits with high activity in the UV range, such as diazirine derivatives. In the following patterning approach, we photoimmobilized a diazirine-alkyne linker on commercially available, hydrogel-passivated μ-Slides (μ-Slide IV$^{0.4}$ Bioinert, ibidi GmbH) and subsequently functionalized the linker with a cyclic RGD-azide (Figure S2B,C).

With this setup, the patterning of large areas is feasible and was used to generate adhesion arrays of single cell-sized (35 μm) and multicell-sized (200 μm) adhesion pads within a passivated flow channel (Figure 4A). Cell seeding in the channel system results in a very homogeneous distribution of cells on the pattern due to the laminar flow conditions within the microchannel. The high reactivity and short lifetime of the activated diazirine-alkyne linker in combination with a photomask-based illumination allow for a patterning with very low unspecific binding of the linker molecule in the nonilluminated areas. This restricts cell adhesion to the patterned spots, even if grown beyond confluency to grow spheroids (Figure 4A, large spots) or if cultured over more than 2 weeks on complex pattern geometries (Figure S2D).

To quantify the patterning contrast, we used a Cy3-azide ligand to visualize the structures and compare the diazirine immobilization with patterns generated with a 6-FAM linker

https://doi.org/10.1021/acsami.1c09850
ACS Appl. Mater. Interfaces 2021, 13, 35545−35560

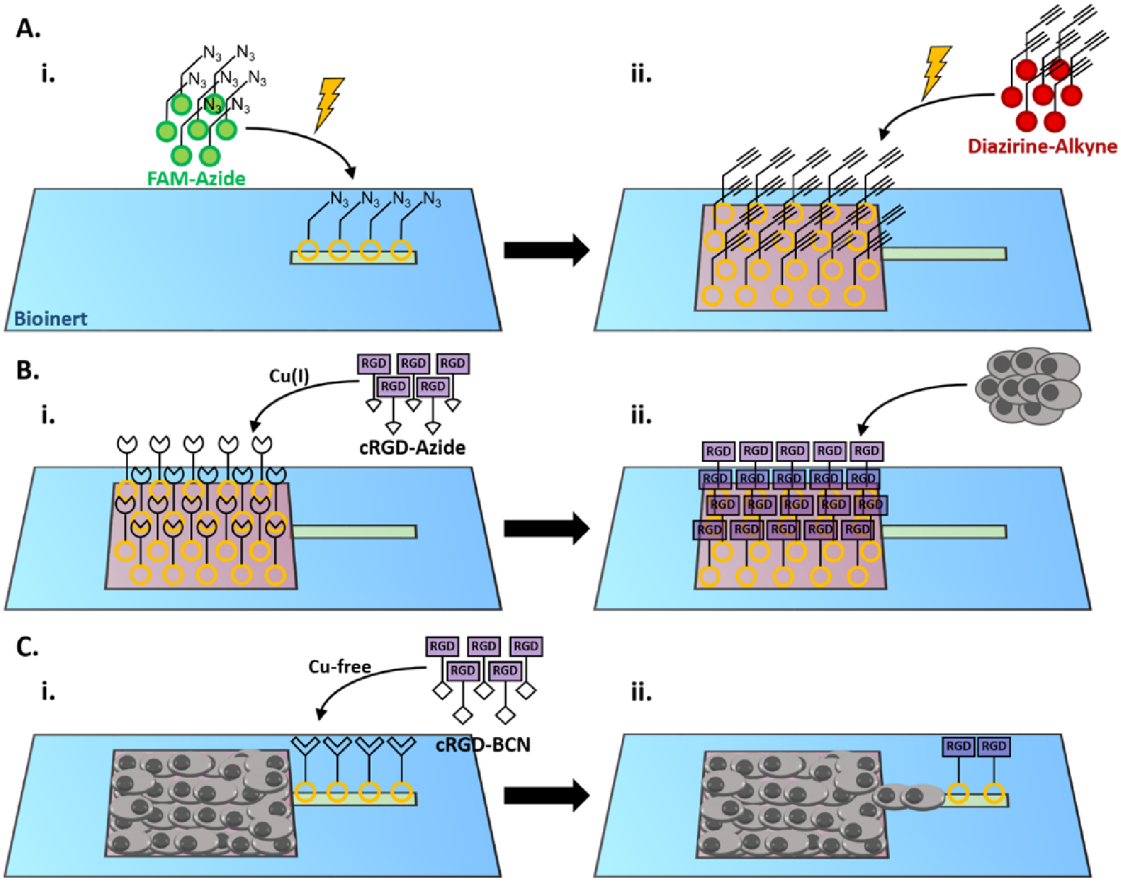

Figure 6. Detailed illustration of the photobleaching process and click chemistry reactions to produce sequentially cell-adhesive areas. (A) Photobleaching for creating the tip and stalk area. (i) 6-FAM-azide conjugates (left), which, upon illumination through the lines left uncovered by the first mask, attach to the surface (right). (ii) Diazirine-alkyne conjugates (right), which, upon illumination through the squares left uncovered by the second mask, attach to the surface (left). (B) Click chemistry reaction for activation of the stalk areas. (i) Addition of the first click reaction solution containing RGD peptides with azide functional groups. The azide groups form triazole links with the alkyne groups of the diazirine-alkyne conjugates that are already attached to the square areas. These areas are now activated with RGD and adhesive to cells. (ii) HMECs are seeded on the square areas forming the initial stalk cell population. (C) Click chemistry reaction for activation of the tip areas. (i) Addition of the second click reaction solution containing RGD peptides with BCN functional groups. The BCN groups link to the azide groups of the 6-FAM-azide conjugates that are already attached to the line areas. These areas are now also activated with RGD and adhesive to cells (timepoint 0). (ii) Endothelial cells from the stalk areas migrate to the tip areas.

and illumination with a 470 nm collimated LED (Figure 4B). Very high signal-to-noise ratios can be generated with the diazirine setup with a more than 3-fold increase of the signal-to-background ratio compared to the 6-FAM pattern (Figure 4C). Diazirine not only produces lower background but also shows a distinct drop of Cy3 fluorescence intensity at the edge of the pattern in contrast to the 6-FAM linker (Figure 4D). Due to the absence of a conjugated pi-electron system within the diazirine-alkyne linker, the pattern does not have any inherent fluorescence (Figure 4E) and therefore background-free fluorescent live-cell imaging or immunofluorescence readouts are possible (Figure 4F).

This high-throughput photopatterning approach has several advantages compared to existing photopatterning methods that implement microfluidics (i.e., ref 53). First of all, it allows for single-cell and cell colony experiments, providing the ability of performing multiple tests at a time. Second, the current setup has the capacity to be extended to generate areas of different geometries that can be treated independently, offering spatiotemporal control to the experimenter. This extension of the method is described in the following paragraphs.

Transition from Single to Sequential Photopatterning to Generate a "Dynamic" System for Studying the Tip/Stalk Phenotype Switch in Angiogenesis. After the successful application of our building-block-based single photopatterning method to confine growth and migration of cells to designated areas and gradients, this technique was further developed to allow sequential patterning. An important requirement was the temporal control of the spatial patterning. We thus introduced the capacity to pattern neighboring geometries with different functionalities. We then added the feature of activating the patterns at defined times during the experiment. We refer to this expanded method as sequential photopatterning. We assessed the applicability of our sequential photopatterning by employing a more complex cellular process, namely, the tip/stalk cell phenotype switch of endothelial cells during angiogenesis. During this process (the production of new blood vessels from the pre-existing ones), endothelial cells differentiate into two different populations, the tip and the stalk cells,[54] which are characterized by specific marker proteins. The tip cells act as guides of the sprouting blood vessel, while the stalk cells follow the leading tip cells, comprising the base of the sprout.[55] Two main factors are

https://doi.org/10.1021/acsami.1c09850
ACS Appl. Mater. Interfaces 2021, 13, 35545−35560

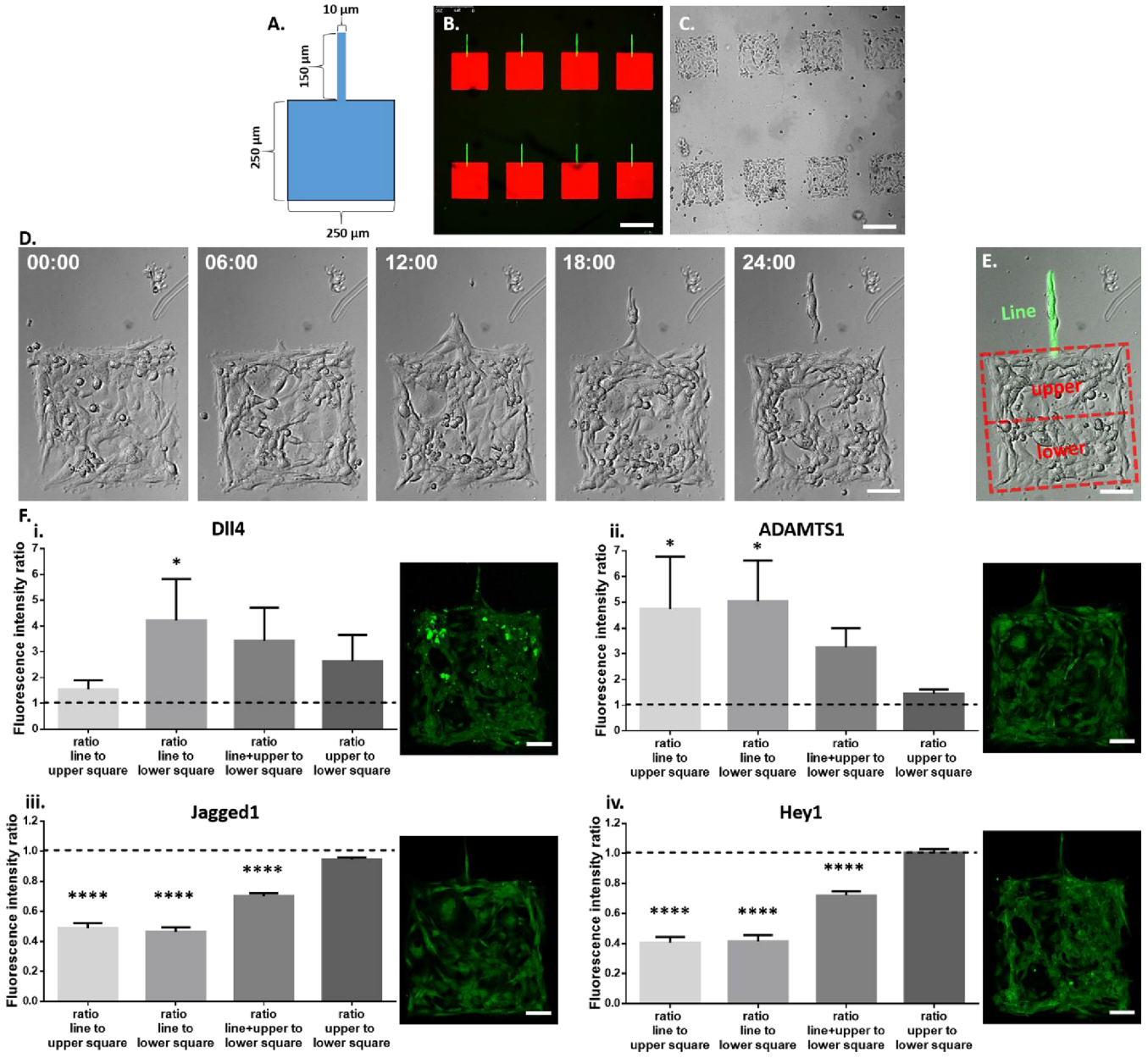

Figure 7. Cell adhesion on the "dynamic" system created by sequential photopatterning and evaluation of tip/stalk protein marker expression. (A) Schematic illustration of the geometry and dimensions of the "dynamic" system generated using sequential photopatterning. (B) Confocal images of diazirine-patterned square areas labeled with DBCO-Sulfo-Cy5 (red) and residual intensity of 6-FAM-patterned line areas (green). Scale bar: 250 μm. (C) Bright-field microscopy image of HMECs adhering on the patterned surfaces. (D) Time lapse of cell migration to the tip. (E) Overlay of the bright-field microscopy image and the fluorescence microscopy image showing the residual fluorescence of the line area (green). The red dashed outline shows the upper and lower square (stalk) compartments, and the green fluorescent line shows the line (tip) compartment. (F) Left panels: Quantitative analysis of the expression of the tip-related markers Dll4 (i) and ADAMTS1 (ii) and the stalk-related markers Jagged1 (iii) and Hey1 (iv). Here, for each marker, the fluorescence intensity ratios between the different compartments of the patterned area (line, upper square, line + upper square, lower square) were determined. Bars represent the mean ratios of the "dynamic" system +SEM. Statistical significance was assessed using one-way ANOVA followed by uncorrected Fisher's LSD test. (i) Dll4: line/upper$_{mean}$ = 1.54, p = 0.71; line/lower$_{mean}$ = 4.2. p = 0.03; line + upper/lower$_{mean}$ = 3.42, p = 0.1; and upper/lower$_{mean}$ = 2.63, p = 0.27 (n = 9). (ii) ADAMTS1: line/upper$_{mean}$ = 4.74, p = 0.03; line/lower$_{mean}$ = 5.03, p = 0.02; line + upper/lower$_{mean}$ = 3.24, p = 0.19; and upper/lower$_{mean}$ = 1.44, p = 0.79 (n = 7). (iii) Jagged1: line/upper$_{mean}$ = 0.49, p < 0.0001; line/lower$_{mean}$ = 0.46, p < 0.0001; line + upper/lower$_{mean}$ = 0.70, p < 0.0001; and upper/lower$_{mean}$ = 0.94, p = 0.08 (n = 15). (iv) Hey1: line/upper$_{mean}$ = 0.40, p < 0.0001; line/lower$_{mean}$ = 0.41, p < 0.0001; line + upper/lower$_{mean}$ = 0.72, p < 0.0001; and upper/lower$_{mean}$ = 1.00, p = 0.90 (n = 24). n.s.: nonsignificant, *p < 0.05, and ****p < 0.0001. Right panels: Exemplary fluorescence microscopy images of cells stained for the corresponding marker that is quantified in the left panel. Scale bar: 50 μm.

considered responsible for inducing the tip/stalk phenotype switch: the shape change that endothelial cells undergo during relocation and the process of directed migration toward a target area. Our sequential photopatterning system can control both features, as the time-controlled activation (chemically induced cell adhesiveness) of the narrower patterned areas enables directed cell migration from the wider to the narrower adhesive areas. This we refer to as a "dynamic" system.

https://doi.org/10.1021/acsami.1c09850
ACS Appl. Mater. Interfaces 2021, 13, 35545−35560

The selected pattern geometries of our "dynamic" system comprised large 2500 μm squares and narrow 10 μm wide, 150 μm long lines (Figures 5−7A). We started the process of photopatterning by utilizing the previously discussed hydrogel-coated Bioinert foil from ibidi (Figures 1C and 5A(iv)), which prevents the adhesion of proteins or cells. Similar to our single photopatterning process, we produced the adhesive areas by photobleaching and click chemistry, this time using a photosensitive fluorescent dye conjugated with an azide functional group (6-FAM-azide, ex. 488 nm, Figures 5A(iii) and 6A(i)). A custom-made chromium mask (Figure 5A(i)) left defined areas in a line-patterned manner exposed, allowing the selective photobleaching of the 6-FAM dye through the exposed line areas upon strong illumination with a collimated 470 nm LED (Figure 5A(v)). The resulting pattern of azide-covered lines will be referred to as tip areas. Following that, a second chromium mask (Figure 5B(i)) was used on the line-patterned surface, which left defined 2500 μm square areas exposed. This allowed the selective photobleaching of a different dye linker (diazirine-alkyne, ex. 350 nm, Figures 5B(iii) and 6A(ii)) through the exposed square areas upon illumination with a 360 nm collimated LED, resulting in a pattern of alkyne-covered squares (will be referred to as stalk areas) (Figure 5C(i)). The use of a custom-made realigner that includes crossover square alignment markers (Figures 5A-A(ii),B(ii) and S3) was essential to precisely align the line and square patterns during illumination (Figure 5B(v)) with micrometer accuracy. This ensures that each line is connected to the middle of the right side of each square, resulting in the desired stalk/tip pattern (Figures 5C and 7B). High accuracy in alignment was not trivial, as misaligned patterns could alter the outcome of our experiment.

This photolithography process was followed by two different sequential click chemistry reactions that finally rendered the aforementioned patterned areas cell adhesive. For the addition of the click chemistry reaction solutions as well as the subsequent cell seeding on our foils, the attachment of an 8-well bottomless μ-Slide to the patterned surface was required (Figure 5C(ii)). The first functionalization step was the copper-catalyzed reaction between the alkyne groups on the square areas and the azide groups of RGD-azide peptides that were added to the click reaction solution (Figure 6B(i)). This enabled the following selective adhesion of HMECs only on the RGD-containing square areas, forming the initial stalk cell population (Figures 6B(ii) and 7C). At timepoint 0, the copper-free click reaction between the azide linker groups on the line areas and the BCN groups of the newly added RGD-BCN peptides took place (Figure 6C(i)). This resulted in the activation of the tip areas (Figure 6C(ii)), as they became cell adhesive, and was considered the starting point of cell differentiation.

According to our observations, ∼16 h after the tip area activation, the cells in most of the patterns had already migrated halfway along the tip (representative time lapse in Figure 7D). Eventually, at 24 h after activation, all patterns had fully covered tip areas and the migration was complete (Figure 7E). As expected, cells were confined in the patterned areas throughout the experiment, verifying the spatial control of our method. More importantly, the ability to initiate migration at a chosen timepoint verified the temporal control provided by our approach.

To assess whether a phenotypic switch took place between cells in the tip and stalk areas, we fixed the cells at 16 h postactivation and used immunohistochemistry to visualize the levels of protein markers corresponding to each phenotype. More specifically, we visualized proteins that are known components of the Notch signaling pathway, namely, Hey1/Jagged1 associated with the stalk phenotype and Dll4/ADAMTS1 related to the tip phenotype.[56] For each of the aforementioned markers, we calculated the fluorescence intensity ratio between the tip (line) and stalk (upper or lower square) compartments (Figure 7F). The upper half of the square was considered as an intermediate compartment where some cells might transition from the stalk to tip phenotype. Regarding the known tip cell markers Dll4 (Figure 7F(i)) and ADAMTS1 (Figure 7F(ii)), we found that their fluorescence intensity was 4.21 and 5.03 times higher, respectively, in the line compartment compared to the lower square compartment ($p < 0.05$). Moreover, the intensity of ADAMTS1 also showed a 4.74-fold increase in the line compartment compared to the upper square compartment ($p < 0.05$), which was not the case for Dll4. However, for both tip markers, there was no significant difference in the fluorescence intensity between the upper and lower square or line + upper to lower square compartments, as shown by the corresponding calculated ratios (Figure 7F(i,ii)). Therefore, the expression of the tip markers Dll4 and ADAMTS1 is strongly associated with our designated tip area. On the other hand, for the stalk marker Jagged1 (Figure 7F(iii)), the fluorescence intensity was 2.04- and 2.17-fold lower in the line compartment compared to the upper and lower square compartments, respectively ($p < 0.0001$). In addition, this marker showed a 1.4-fold intensity reduction in the line + upper square compared to the lower square compartment ($p < 0.0001$). Our fluorescence intensity measurements of the Hey1 stalk marker (Figure 7F(iv)) exhibited similarities with the Jagged1. More specifically, the Hey1 fluorescence intensity was 2.5 and 2.4 times lower in the line compartment compared to the upper and lower square compartments, respectively ($p < 0.0001$). Moreover, Hey1 had a 1.38-fold drop in the fluorescence intensity inside the line + upper square areas compared to the lower square compartment ($p < 0.0001$). For both stalk markers, fluorescence intensity comparisons between the upper and lower square compartments showed no significant differences. Thus, the expression of the stalk markers Jagged1 and Hey1 is associated with our designated stalk areas and even more so to the lower square compartment, which is more clearly a "stalk" compartment, being further away from the tip area. These findings show that our "dynamic" system was efficient in inducing a predominance of the tip cell phenotype in the tip area and the stalk cell phenotype in the stalk area, verifying its applicability in studying dynamic cellular behavior.

Comparison between "Dynamic" and a Control "Static" System. We then moved on to comparing the "dynamic" system with a control "static" system that can induce a similar shape change but does not allow for time-controlled directed migration. This "static" system was generated using standard microcontact printing as described previously[15,57] and involved the same patterned geometries as the "dynamic" system (Figure S4). We found that the "static" system was able to induce an increase in the Hey1 mRNA expression in the square compared to the line compartment (Figure S4, detailed description of mean differences and p values is given in Tables S1 and S2) This was a first indication that the cell-shape change induced by the different surface geometries affected the tip-stalk "status" of the endothelial cells on the level of gene

https://doi.org/10.1021/acsami.1c09850
ACS Appl. Mater. Interfaces 2021, 13, 35545−35560

expression. To further investigate a possible phenotypic switch, we calculated the tip and stalk protein marker fluorescence intensity ratios between the line and the square compartments, as we did for our "dynamic" system. In the case of the tip marker Dll4 (Figure S5D(i)), its fluorescence intensity was 1.21-fold higher in the upper compared to the lower square compartment ($p < 0.01$), but no significant differences in intensity were observed between the other compartments. With regard to the tip marker ADAMTS1, the intensity was 1.38 times higher in the line compared to the lower square compartment ($p < 0.05$), while no significant difference between the other compartments was observed (Figure S5D(ii)). On the contrary, for the stalk markers Jagged1 and Hey1, there was no significant variation in their intensity between the different compartments (Figure S5D(iii,iv)). The small increase in the ADAMTS1 marker expression in the line compared to the lower square compartment shows that the shape change factor alone can slightly promote a tip phenotype in the tip area. The Dll4 marker was less specific for the designated tip area, being slightly increased in the upper square, in proximity to the line compartment but not inside it. Furthermore, the lack of significant difference in both stalk marker expression between the tip- and stalk-designated areas suggests that the cell-shape change factor is less efficient in inducing a robust and complete tip-stalk phenotype switch when the directed migration component is missing.

Direct comparison between the two systems revealed that the "dynamic" system was significantly more sensitive compared to the "static" system in identifying differences in the expression levels of all markers between the different compartments, here expressed as the ratios of their fluorescence intensities (Figure S6). The increased sensitivity of the "dynamic" system in detecting such differences compared to the "static" system can be attributed to the factor of directed migration, which only the "dynamic" system provides in addition to the shape change factor that both systems incorporate. Such a "dynamic" system that allows time-controlled directed migration is required to fully and reliably model "dynamic" processes.

CONCLUSIONS

In this study, we introduce a building-block-based covalent photopatterning technique that stands out due to its robustness and versatility in using different linkers, ligands, and illumination systems, tailored to the biological application needed. Using sequential illumination steps with different linkers and functionalization of the created structures in the presence of cells, complex dynamic cell processes, such as, e.g., tip/stalk cell switch in angiogenesis, can be mimicked. The efficacy of our system in imitating such a process underscores the experimental advantage of achieving temporal as well as spatial control over the cell microenvironment in vitro, suggesting that this setup could be adapted to answer various biological questions.

MATERIALS AND METHODS

Patterning Methods. *PVA Coating.* Glass bottom dishes (MaTek, USA) were PVA coated as described earlier.[43] Briefly, the glass surface of MaTek dishes was activated for 25 min at room temperature with 50% nitric acid (Sigma-Aldrich, St. Louis, MO). After activation, the dish was rinsed overnight with ddH_2O. Subsequently, the glass surface was deprotonated by incubation for 15 min at room temperature with 200 mM NaOH (Sigma-Aldrich, St. Louis, MO). The deprotonated and washed glass surface (ddH_2O) was blow-dried using canned nitrogen. By incubation with 1% aqueous solution of APTES (w/v, Sigma-Aldrich, St. Louis, MO), the glass surface was amino-silanized for 5 min and carefully washed with ddH_2O for 10 min. The amino-silanized glass surface was then cured at 65 °C for 3 h. For aldehyde activation, surfaces were incubated with 0.5% aqueous glutaraldehyde (Sigma-Aldrich, St. Louis, MO) solution for 30 min at room temperature. An ∼200 nm thick poly-vinyl alcohol (PVA, 6% aqueous solution with 0.1% 2N HCl) film was bound to the glutaraldehyde-activated surface by spin coating (40 s at 7000 rpm; 550 rpm acceleration within 18 s). Prior to use, the dishes were washed carefully with ddH_2O.

Photoimmobilization of 6-FAM-Alkyne with a Pulsed UV Laser. Approximately 20 μL of 6-FAM-alkyne (Lumiprobe, Hannover, Germany) was placed in the middle of a PVA-coated glass dish, and patterns were written using a steerable, pulsed UV laser (λ = 355 nm) as described before.[8] Briefly, the UV laser was focused into the interface between the bottom of the PDMS-coated glass slide and the 6-FAM-alkyne solution with a long working distance 20× objective (Zeiss LD Plan Neo 20× 0.4). A pair of high-speed galvanometric mirrors, controlled by a custom program, moved the focal spot within the 6-FAM-alkyne droplet.

The gradient pattern was specified by an image whose pixel values determined the light dose used for bleaching. Careful calibration allowed compensating for the off-center drop-off of the numerical aperture of the objective as well as the geometric distortions from the imperfect imaging of the scan mirrors into the back aperture of the objective. This allowed gradient writing in the full field of view of the objective. For each spot, the total light dose was split up into multiple laser pulses to average out the pulse-to-pulse power variability of the laser. The gradient was written one spot at a time with the scanning mirrors moving the laser focus by about half the diameter of the focus spot to create a continuous pattern. In this way, crosstalk between different locations in the pattern was minimized since the scattered light from one spot did not reach the threshold of bleaching elsewhere unlike projector-based systems where the entire area is exposed simultaneously. The low wavelength of the UV laser leads to a high lateral resolution (∼0.7 μm) and the low crosstalk to a high dynamic range (∼100:1) of the gradient pattern. The writing speed was limited by the laser's pulse frequency of 1 kHz. A full description of the hardware employed can be found in the study by Behrndt et al.[58]

Photoimmobilization of 6-FAM-Alkyne with Projector-Based Photopatterning. Projector-based photopatterning was accomplished using a microscope-coupled LCD projector similar to the one designed by Stirman et al.[59] Briefly, the light source of an LCD-based overhead projector (Panasonic PT AE6000E; contrast ratio of 297 ± 1:1) is replaced by a 470 nm LED source (Thorlabs M470L3). The projection lens is removed, and the projected image is coupled with a relay lens (Thorlabs AC508-100-A-ML, f = 100 mm) into the rear port of an Olympus IX83 inverted microscope. A 50/50 beamsplitter (Thorlabs BSW10R) directs half of the incident light through a 20× objective (Olympus LUCPLFLN20XPh) to the substrate surface. The reflection of the projected pattern from the substrate−air interface is imaged on a digital camera (Hamamatsu Orca Flash4.0v2). With the microscope focused on the substrate surface, the projector is adjusted to bring the projected image and microscope focal planes into alignment. Custom software utilizing MATLAB and MicroManager[60] is used to generate and project patterns and to control LED illumination and the microscope. When exposing patterns, a prepared substrate is washed and dried by aspiration before mounting securely on the microscope's stage. The microscope focus is then adjusted to bring a projected target pattern into focus at the substrate surface. When multiple patterns are to be exposed on a single substrate, focal offsets are manually determined at the extremities of the pattern array and offsets at intermediate locations estimated by least-squares fitting of a plane through the measured points. The LED is extinguished, and a small volume of 6-FAM-alkyne is carefully deposited onto the target surface without displacing the substrate. The system then automatically cycles sequentially through the pattern locations, at each exposing specified pattern for corresponding durations.

https://doi.org/10.1021/acsami.1c09850
ACS Appl. Mater. Interfaces 2021, 13, 35545−35560

1,3 Dipolar Cycloaddition of RGD-HF555 in Single Photopatterning. GRGDS-HF555-azide (RGD-HF555) was custom synthesized by Eurogentec (Serain, Belgium). Following laser writing or projector-based patterning, the alkyne-patterned PVA surfaces were washed with PBS and incubated for 30 min in the dark with the reaction mixture (Table 5). After washing with PBS, RGD-HF555 patterns can be stored for up to a month under PBS.

Table 5. Click Reaction Mixture

volume (μL)	component	concentration in reaction
2.2	click-iT cell reaction buffer (Thermo)	
19.8	ddH_2O	
2.5	reaction buffer additive (Thermo)	
0.5	$CuSO_4$	8.3 mM
5	RGD-HF555 (stock 180 μM)	30 μM

High-Throughput Photopatterning with a Collimated LED. ibidi μ-Slides $VI^{0.4}$ Bioinert were used as a cell-repellent background for high-throughput patterning with a collimated LED. To each channel, 24 μL of the linker solution (either 0.9 mM 6-FAM-alkyne (Jena Bioscience, Germany) in PBS or 1.5 mM diazirine-alkyne (custom synthesis from Enamine, Ukraine) in MilliQ water) is injected. The slide is put on a chromium mask (Compugraphics, Germany), which contains the desired structures to shield the designated nonadherent areas from light exposure. The mask with the slide is put on an upward-facing collimated LED of fitting wavelength: for 6-FAM-alkyne 470 nm LED (Thorlabs, Germany) and for diazirine-alkyne 380 nm (Rapp OptoElectronic, Germany) and illuminated for 5 min at maximum intensity (6-FAM-alkyne) or for 1 min at 40% intensity (diazirine-alkyne). After illumination, channels are washed six times with Milli-Q water to get rid of the unbound linker.

1,3 Dipolar Cycloaddition of cRGD or Sulfo-Cy3 in High-Throughput Photopatterning. After immobilization of the linker as described in the previous chapter, the linker is either functionalized with a sulfo-Cy3-azide (Lumiprobe, Germany) for pattern visualization or with cyclic-RGD-azide (cRGDfK, Peptides International, USA) for cell adhesion studies. For both reactions, the same conditions are used (Table 6). First, $CuSO_4$ (Jena Bioscience, Germany) is mixed with BTTAA (Jena Bioscience, Germany). Then, the buffer, azide and ascorbic acid (Jena Bioscience, Germany), is added and mixed thoroughly. The reaction mixture (25 μL) is directly pipetted into each channel after mixing and incubated for 1 h in the dark. The channels are afterward washed multiple times with MilliQ water, and after another washing step overnight, the channels are emptied and dried by an air stream.

Table 6. Click Reaction Mixture for a μ-Slide $IV^{0.4}$ Volume (25 μL/channel) Used in the High-Throughput Photopatterning Protocol

volume (μL)	component (stock concentration)	assay concentration
15	sulfo-Cy3-azide or cRGD-azide (2 mM)	200 μM
30	BTTAA (50 mM)	10 mM
15	ascorbic acid (1 M)	100 mM
3	$CuSO_4$ (100 mM)	2 mM
87	100 mM sodium phosphate buffer (pH 8.0)	

Fabrication of an Aluminum Realigner. A custom-made aluminum realigner was designed using drawing software, e.g., autocad (Autodesk) or CircuitPro PL (LPKF Laser & Electronics, Germany), to the size and dimension necessary to accommodate the collimated LEDs and Bioinert foils used. The fabrication was performed in the Chemistry and Pharmacy Precision Mechanics Workshop using a single slab of aluminum and the appropriate precision machines. The exact dimensions as well as a detailed visual representation is provided in Figure S5.

Fabrication of Chromium Mask Masters. The desired patterns can be designed using a drawing software, e.g., AutoCAD (Autodesk) or CircuitPro PL (LPKF Laser & Electronics, Germany). Masters for stamp preparation or masters for photopatterning experiments can then be created by following established protocols (such as those provided by photoresist producers like MicroChem) or the protocol provided in Supplementary Methods in the Supporting Information. Note that labs that do not have the means to create stamp masters can order them online (from HTS Resources, for example). Once prepared, each master can be used to make multiple stamps or multiple surface photopatterning experiments.

Sequential Photopatterning. For the photopatterning of tip areas, we used the first chromium mask produced as described above, etched in a line-patterned manner, with cross-shaped alignment markers on either side of the main patterns. The mask was placed on the custom-made realigner, and 50 μL of a 2 mM 6-FAM-azide dye linker (Lumiprobe Corporation, USA) solution in PBS was added at the center of the mask and then carefully covered by ibidi's Bioinert foil so that the liquid spreads homogeneously on the surface. Upon a maximum illumination of 7 min, from underneath, with a 470 nm collimated LED (Thorlabs, Germany), the line pattern was produced on the foil's inner surface and the foil was removed from the realigner, as was the first chromium mask. The foil was then submerged for 5 min in a Petri dish with PBS (pH 8.5), and the mask was submerged for 5 min in a separate Petri dish with the same buffer. Then, the foil was submerged for 5 min in a new PBS (pH 8.5) solution and the mask for 5 min in a new ethanol (99%, Sigma-Aldrich, USA) solution. Finally, the foil was submerged one last time for 5 min in a MilliQ solution and then together with the mask dried in a nitrogen stream and left at room temperature for 30 min. For the photopatterning of the stalk areas, we used a second chromium mask etched in a square-patterned manner, with square-shaped alignment markers on either side of the main patterns. The second mask was placed on the realigner, and 50 μL of 10 mM diazirine-alkyne dye linker in PBS (Sigma-Aldrich, USA) solution was added at the center. As the tip-patterned foil was positioned on top, the crossover square alignment markers were used to precisely align the foil's existing line pattern with the square pattern of the second mask. In all cases, the precise alignment was performed under a microscope at 10× magnification (EVOS FL Cell Imaging System, Life Technologies, USA). This second mask-dye-foil configuration was illuminated, from underneath, for 5 min with a 360 nm collimated LED (Rapp OptoElectronic GmbH, Germany), resulting in the final line (tip) and square (stalk) photopatterned surface on the Bioinert foil. Next, the foil and the second mask were washed again following the previously described multistep washing protocol. As a next step, an adhesive 8-well

Table 7. Click Reaction Mixture for an 8-Well Slide Volume (15 μL/Well) Used in the Sequential Photopatterning Protocol

volume (μL)	component (stock concentration)	assay concentration
36	cRGD-azide (2 mM) or DBCO-sulfo-Cy5 dye (1 mM)	600 μM cRGD-azide or 70 μM DBCO-sulfo-Cy5 dye
20	BTTAA (50 mM)	10 mM
14	ascorbic acid (1 M)	100 mM
6	$CuSO_4$ (100 mM)	2 mM
44	100 mM sodium phosphate buffer (pH 8.0)	

https://doi.org/10.1021/acsami.1c09850
ACS Appl. Mater. Interfaces 2021, 13, 35545−35560

bottomless μ-Slide (sticky-Slide 8 Well, ibidi GmbH, Germany) was attached on the patterned surface of the foil. We continued with the addition of click reaction solutions starting with the addition of 15 μL of the click reaction solution (Table 7) containing azide-RGD peptides at the center of each well, with an 8 × 8 mm^2 glass coverslip (H. Saur Laborbedarf, Reutlingen, Germany) above them, and allowed them to react for 2 h. During this time, the azide groups on the RGDs formed triazole links with the alkyne groups of the diazirine-alkyne conjugates that were already attached to the square areas. As a result, these areas were now activated with RGD and therefore adhesive to cells. At this point, HMECs were trypsinized after reaching confluency and diluted to the desired density (170 000 cell/mL) in endothelial cell growth medium and 250 μL of this cell suspension was added into each well and allowed to settle overnight at 37 °C, forming the initial stalk cell population on the square areas. Following that, cells were gently washed 1× with the medium and 200 μL of new medium was added into each well. Then, for the second click reaction solution, 5 μL of 100 μM BCN-cRGDfk (Synaffix, the Netherlands) in PBS was added into the medium of each well to a final concentration of 10 μM. The BCN groups formed a link with the azide groups of the 6-FAM-azide conjugates that were already attached to the line areas, and as a result, these areas were now also activated with RGD and thus adhesive to cells (timepoint 0).

Cell Culture and Primary Cells. Swiss 3T3 mouse fibroblasts were maintained in high-glucose Dulbecco's modified Eagle's medium (DMEM + GlutaMAX) supplemented with 1% penicillin, 1% streptomycin, 1% glutamine, and 10% fetal bovine serum (Gibco Life Technologies) at 37 °C.

Zebrafish used in this study was bred and maintained according to the Austrian law for animal experiments ("Österreichisches Tierschutzgesetz"). For preparation of keratocytes, scales from wild-type zebrafish (strain AB) were transferred to plastic cell culture dishes containing start medium as described previously (Anderson, K. S.; Small, J. V. Preparation and fixation of fish keratocytes. Cell Biology: A Laboratory Handbook, Vol. 2, 372−376 (Academic, 1998)). After 1-day incubation at 28 °C, monolayers of cells were treated with 1 mM EDTA in running buffer for 45−60 min to release individual cells.

NIH-3T3 mouse fibroblasts were maintained in DMEM (Gibco Life Technologies) supplemented with 4 mM L-glutamine (Gibco Life Technologies) and 10% bovine calf serum (Gibco Life Technologies) at 37 °C and 5% CO_2.

RCC26 renal cell carcinoma cells are maintained in RPMI (Gibco Life Technologies) supplemented with 10% FCS (Gibco Life Technologies), 1% MEM (nonessential amino acid solution, Sigma-Aldrich), and 1% sodium pyruvate (Gibco Life Technologies) at 37 °C and 5% CO_2.

Human microvascular endothelial cells (HMECs) were purchased from ATCC and maintained in endothelial cell growth medium containing 10% fetal calf serum (FCS), 10 000 U/mL penicillin/streptomycin, and 250 mg/mL amphotericin B under constant humidity at 37 °C and 5% CO_2. Experiments were performed using cells at passage 6.

Adhesion Assays and Migration Assays. *3T3 Fibroblasts.* Confluent 3T3 fibroblasts were detached with 0.05% trypsin-EDTA. Depending on the experiment, 10^4−10^5 cells were plated onto GRGDS-functionalized coverslips and incubated for 3−4 h at 37 °C to allow for attachment. Prior to recording on the microscope, unattached cells were removed by gentle washing with medium.

Zebrafish Keratocytes. EDTA-released zebrafish keratocytes were washed with PBS, detached with 0.05% trypsin-EDTA, and replated on GRGDS-functionalized coverslips. After 30 min of incubation at RT, nonattached cells were washed away.

RCC Cells and NIH-3T3. Subconfluent cells were detached using trypsin/EDTA solution. Depending on the experiment, 2.5−4 × 10^5 cells/mL in culture medium were flushed into the channels of a μ-Slide $VI^{0.4}$. Excess solution was removed, leaving only the channels filled. The reservoirs were directly filled with culture medium, and the slide was incubated overnight at 37 °C. The next day, the cell culture medium was carefully exchanged to wash away unattached cells. For long-term cultivation, cells were incubated at 37 °C and cell culture medium was exchanged every 2−3 days.

Immunohistochemistry. *Antibody and Staining Reagents for High-Throughput Patterning Experiments.* Antibodies used to stain RCC26 cells were mouse antialpha-tubulin antibody (diluted 1:1000, Sigma-Aldrich) in combination with antimouse IgG-Atto594 (end concentration of 2 μg/mL, Sigma-Aldrich). To stain for actin and the nucleus, DY-490-Phalloidin (1:500, Dyomics) and DAPI (1 μg/mL, Sigma-Aldrich) were used, respectively.

Cells were fixed by exchanging the cell culture medium with 10% neutral buffered formalin solution (Sigma-Aldrich, Germany) and incubated for 10 min at room temperature. Channels were washed 6× with PBS and subsequently incubated with 0.5% Triton X-100 in PBS (Sigma-Aldrich) for 15 min at room temperature. After washing with PBS, 30 μL of primary antibody solution was pipetted into each channel and incubated overnight at 4 °C. After washing 6× with PBS for 5 min, a mixture of secondary antimouse antibody, phalloidin, and DAPI in PBS was injected into the channels and incubated for 3 h at room temperature in the dark. After a final washing step with 6× PBS for 5 min, the cells were ready for imaging.

Fluorescence imaging of stained cells was performed on a Nikon Eclipse Ti, fluorescence microscope (Nikon, Germany) equipped with a Plan Apo 60X/1.4 oil objective (Nikon, Germany) and an Orca Flash 4.0 LT camera (Hamamatsu Photonics, Japan).

Antibodies and Staining Reagents for Tip/Stalk Experiment. The primary antibodies used in this study were raised against ADAMTS1 (3C8F4) mouse mAb IgG_{1k}, sc-47 727 (Santa Cruz Biotechnology, Dallas, TX); Dll4 (G-12) mouse mAb IgG_{2a}, sc-365 429 (Santa Cruz Biotechnology, Dallas, TX); HEY1 rabbit pAb, ab22614 (Abcam, Cambridge, UK); and Jagged1 rabbit pAb, ab7771 (Abcam, Cambridge, UK). The following secondary antibodies were used for this study: Alexa Fluor 488-conjugated goat antimouse IgG (H + L), A-11 001 and Alexa Fluor 647-conjugated chicken antirabbit IgG (H + L), A-21 443. Hoechst 33342 (Sigma-Aldrich, St. Louis, MO) was applied in a dilution of 1:100 with an end concentration of 5 μg/mL. The FluorSave Reagent mounting medium was purchased from Merck Millipore (Darmstadt, Germany).

Immunofluorescence Staining of Tip/Stalk Experiment. Immunofluorescence staining was performed 16 h after activation of the pattern. For immunofluorescence staining, cells were briefly washed with PBS with Ca^{2+} and Mg^{2+}. Subsequently, cells were fixed with 4% methanol-free formaldehyde solution (Themo Fisher, Waltham, MA) for 10 min, washed with PBS, permeabilized with 0.2% Triton X-100 (Roth, Karlsruhe, Germany) in PBS for 10 min, and again washed with PBS. Unspecific binding sites were blocked with 1% BSA (Sigma-Aldrich, St. Louis, MO) in PBS for 30 min at room temperature. For double staining, cells were incubated with the primary antibodies diluted in 0.2% BSA in PBS (1:200) overnight at 4 °C. After 3× 10 min of washing with 0.2% BSA in PBS, cells were incubated with the secondary antibodies (1:400) plus Hoechst 33342 (1:100) diluted in PBS for 1 h at room temperature. After 2× 10 min of washing with 0.2% BSA in PBS and 1× 10 min of washing with PBS, samples were sealed with one drop of mounting medium.

Microscopy. *Single Photopatterning Experiments.* Adhesion and migration assays were recorded on a Leica DMIL LED with a 10×/0.22 High Plan I objective. For RGD-HF555 imaging and quantification, images were obtained using 20×/0.8 air and 63×/1.4 oil immersion objectives on a Zeiss Axio Observer microscope equipped with an external light source (Leica).

High-Throughput Photopatterning with a Collimated LED. To compare the immobilization of diazirne-alkyne and 6-FAM-alkyne, patterns were functionalized with sulfo-Cy3-azide and imaged on a Nikon Eclipse Ti fluorescence microscope (Nikon, Germany) equipped with a 10×/0.3 objective (Nikon, Germany) and an Orca Flash 4.0 LT camera (Hamamatsu Photonics, Japan).

To evaluate the autofluorescence of the pattern generated with the two different linkers, patterns that were functionalized with cRGD-azide were imaged on the Nikon Eclipse Ti fluorescence microscope equipped with a 10×/0.3 objective with identical illumination settings.

https://doi.org/10.1021/acsami.1c09850
ACS Appl. Mater. Interfaces 2021, 13, 35545−35560

Images of cells were taken on the Nikon Eclipse Ti fluorescence microscope equipped with a 4×/0.13 or 10×/0.3 objective.

Sequential Photopatterning Experiments. Live-cell imaging was performed using the HMEC-seeded 8-well photopatterned Bioinert slides with an Eclipse Ti inverted microscope (Nikon, Dusseldorf, Germany) with a 4×/10× phase contrast objective and a CCD camera ([DS-Qi1Mc] Nikon, Dusseldorf, Germany). The slides were inserted into a 37 °C heating and incubation system that was flushed with actively mixed 5% CO_2 at a rate of 10 L/h, and the humidity was kept at 80% to prevent dehydration. The cells were imaged in bright-field, and the line patterns were detected at 488 nm wavelength using the integrated fluorescence LED. Time-lapse video microscopy was performed with a time interval of 5 min between images over 24 h.

Imaging of Immunofluorescence Staining in the Tip/Stalk Experiments. Imaging was performed using the Leica TCS SP8 confocal microscope with the LAS X Core software. An HC PL APO CS2 40×/1.30 NA oil objective and hybrid detectors (Leica HyD) and photomultipliers (PMTs) were applied. In sequential scanning mode, the pinhole size was positioned to 1.0 airy units and the pixel size was set to 2048 × 2048. Two frames were obtained for every channel with a frame rate of 0.582 s^{-1}. The following lasers and excitation sources were employed: 405 nm (diode), 488 nm (argon), and 647 nm (argon).

Evaluation of Dye-Linker Immobilization Efficiency. To visualize both patterns and evaluate the immobilization efficiency of the sequential photopatterning we used, for the line patterns, the residual intensity of the 6-FAM-azide dye and for the squares, a DBCO-Sulfo-Cy5 dye (Jena Bioscience, Germany) were used to label the azides on the diazerin-azide-bleached dye via click chemistry (Table 7). Images were taken using a Leica TCS SP8 confocal microscope with HC PL Fluotar CS2 10×/0.3 NA DRY (Leica, Wetzlar, Germany) using LAS X Core software. The argon laser with a wavelength of 488 or 647 nm was used, and the wavelength range of the detector was set between 480−530 and 640−680 nm, respectively. All images were analyzed using the ImageJ version 1.53c[61] software tool.

Cell Tracking and Image Quantification. Single Photopatterning Experiments. For image processing and cell tracking, Fiji[62] and a plugin for manual tracking ("Manual Tracking"[63] were used. Images and tracking data were analyzed using MATLAB 2013 (MathWorks, Inc., USA). Bright-field movies were preprocessed by normalizing the brightness of each frame. Then, the time-averaged median was subtracted to remove nonmotile particles such as dirt, dead cells, etc. from the images. Subsequently, a pixel classifier (Ilastik)[64] was manually trained on one data set to distinguish cell from noncell pixels. The time projection of cell pixels was used to visualize the printed area, and the RGD-HF555 gradient was manually added to the movies as an extra channel. All cells were manually tracked using ImageJ version 1.53c[62] and its plugin for manual tracking (TrackMate). The position of the cells' center was used to determine the concentration by means of the extra channel. The probability density was defined as the number of localizations obtained through the tracking at a specific concentration divided by the total number of localizations.

Quantification of Immobilization Efficiency of RGD-HF555. Fluorescence intensities of a dilution series of RGD-HF555 (0.8, 0.16, and 0.08 ng/mL) were measured in a defined volume of a 12.87 μm high PDMS chamber (4.2×10^{-8} mL; 57.1 μm × 57.1 × 12.87 μm^3) (see the Supplementary Methods in the Supporting Information for chamber production), and a standard curve was calculated (fluorescence intensity = 3.309 ± 0.1144 molecules/μm^2). Fluorescence intensities of patches of surface-immobilized RGD-HF555-azide were measured using the same imaging settings as for the dilution series. Immobilized RGD-HF555 concentrations were calculated from measured fluorescence intensities using the obtained standard curve.

Comparison of Diazirine-Alkyne and 6-FAM-Alkyne Immobilization with High-Throughput Patterning Using a Collimated LED. To evaluate the signal-to-noise ratio (S/N ratio) between the patterned area and the nonilluminated background, images were analyzed using the ImageJ version 1.52i[61] software tool. A line profile in ImageJ across a pattern was normalized to the maximum intensity detected to compare patterns generated with the two different linkers.

Quantification of Immunofluorescence Staining in Tip/Stalk Experiments. Images of immunofluorescence-stained patterns were processed and analyzed using the ImageJ version 1.53c software tool. After images were segmented (Trainable Weka Segmentation tool), the intensities were determined.

Statistical Analysis. Statistical analysis was performed using GraphPad Prism 8. The type of analysis and significant differences are shown in the corresponding figures except for a detailed SmartFlare statistical analysis that is presented in Tables S1 and S2.

■ ASSOCIATED CONTENT

Supporting Information

The Supporting Information is available free of charge at https://pubs.acs.org/doi/10.1021/acsami.1c09850.

Supplementary methods on microcontact printing procedure, SmartFlare experiments, fabrication of chromium mask masters, stamp preparation for microcontact printing, and design and fabrication of the PDMS chamber; schematic illustrations of LCD and LED photopatterning processes and realigner design; fluorescence microscopy images of SmartFlares and corresponding quantitative graphs; bright-field and fluorescence microscopy images of cell adhesion on the "static" system and quantitative graphs of tip/stalk protein marker expression; graphs of comparison between "static" and "dynamic" system in tip/stalk marker expression (PDF)

Five videos for different examples of migrating cells (AVI, AVI, AVI, AVI, and AVI)

■ AUTHOR INFORMATION

Corresponding Authors

Stefan Zahler − *Department of Pharmacy, Center for Drug Research, Ludwig-Maximilians-University Munich, 81377 Munich, Germany;* orcid.org/0000-0002-5140-7287; Email: stefan.zahler@cup.uni-muenchen.de

Michael Sixt − *Institute of Science and Technology Austria (IST Austria), 3400 Klosterneuburg, Austria;* Email: michael.sixt@ist.ac.at

Authors

Themistoklis Zisis − *Department of Pharmacy, Center for Drug Research, Ludwig-Maximilians-University Munich, 81377 Munich, Germany*

Jan Schwarz − *Institute of Science and Technology Austria (IST Austria), 3400 Klosterneuburg, Austria; ibidi GmbH, 82152 Martinsried, Germany*

Miriam Balles − *ibidi GmbH, 82152 Martinsried, Germany*

Maibritt Kretschmer − *Department of Pharmacy, Center for Drug Research, Ludwig-Maximilians-University Munich, 81377 Munich, Germany*

Maria Nemethova − *Institute of Science and Technology Austria (IST Austria), 3400 Klosterneuburg, Austria*

Remy Chait − *Institute of Science and Technology Austria (IST Austria), 3400 Klosterneuburg, Austria*

Robert Hauschild − *Institute of Science and Technology Austria (IST Austria), 3400 Klosterneuburg, Austria*

Janina Lange − *Faculty of Physics and Center for NanoScience, Ludwig-Maximilians-University Munich, 80539 Munich, Germany*

Calin Guet − *Institute of Science and Technology Austria (IST Austria), 3400 Klosterneuburg, Austria*

Complete contact information is available at:
https://pubs.acs.org/10.1021/acsami.1c09850

Author Contributions

#T.Z. and J.S. contributed equally to this work. T.Z., J.S., M.S., and S.Z. designed the study. T.Z., J.S., and M.B. wrote the paper with feedback from all authors. T.Z., J.S., M.B., and M.K. performed the experiments and analyzed data. M.N., R.C., R.H., J.L., and C.G. contributed to the experiments.

Funding

This project was funded by the Deutsche Forschungsgemeinschaft (DFG, German Research Foundation)—Project-ID 201269156—SFB 1032 (Projects B8 and B12). This work was also supported by the Boehringer Ingelheim Fonds and the European Research Council (ERC CoG 724373) and ibidi GmbH.

Notes

The authors declare no competing financial interest.

■ ACKNOWLEDGMENTS

We would like to thank Charlott Leu for the production of our chromium wafers, Louise Ritter for her contribution of the IF stainings in Figure 4, Shokoufeh Teymouri for her help with the Bioinert coated slides, and finally Prof. Dr. Joachim Rädler for his valuable scientific guidance.

■ REFERENCES

(1) Ricoult, S. G.; Kennedy, T. E.; Juncker, D. Substrate-Bound Protein Gradients to Study Haptotaxis. *Front. Bioeng. Biotechnol.* **2015**, *3*, No. 40.
(2) Segerer, F. J.; Thüroff, F.; Piera Alberola, A.; Frey, E.; Rädler, J. O. Emergence and Persistence of Collective Cell Migration on Small Circular Micropatterns. *Phys. Rev. Lett.* **2015**, *114*, No. 228102.
(3) Yoon, S. H.; Kim, Y. K.; Han, E. D.; Seo, Y. H.; Kim, B. H.; Mofrad, M. R. K. Passive Control of Cell Locomotion Using Micropatterns: The Effect of Micropattern Geometry on the Migratory Behavior of Adherent Cells. *Lab Chip* **2012**, *12*, 2391–2402.
(4) Jiang, X.; Bruzewicz, D. A.; Wong, A. P.; Piel, M.; Whitesides, G. M. Directing Cell Migration with Asymmetric Micropatterns. *Proc. Natl. Acad. Sci. U.S.A.* **2005**, *102*, 975–978.
(5) Parker, K. K.; Brock, A. L.; Brangwynne, C.; Mannix, R. J.; Wang, N.; Ostuni, E.; Geisse, N. A.; Adams, J. C.; Whitesides, G. M.; Ingber, D. E. Directional Control of Lamellipodia Extension by Constraining Cell Shape and Orienting Cell Tractional Forces. *FASEB J.* **2002**, *16*, 1195–1204.
(6) Théry, M.; Racine, V.; Piel, M.; Pépin, A.; Dimitrov, A.; Chen, Y.; Sibarita, J.-B.; Bornens, M. Anisotropy of Cell Adhesive Microenvironment Governs Cell Internal Organization and Orientation of Polarity. *Proc. Natl. Acad. Sci. U. S. A.* **2006**, *103*, 19771–19776.
(7) Schiller, H. B.; Fässler, R. Mechanosensitivity and Compositional Dynamics of Cell-Matrix Adhesions. *EMBO Rep.* **2013**, *14*, 509–519.
(8) Bélisle, J. M.; Correia, J. P.; Wiseman, P. W.; Kennedy, T. E.; Costantino, S. Patterning Protein Concentration Using Laser-Assisted Adsorption by Photobleaching, LAPAP. *Lab Chip* **2008**, *8*, 2164–2167.
(9) Gray, D. S.; Liu, W. F.; Shen, C. J.; Bhadriraju, K.; Nelson, C. M.; Chen, C. S. Engineering Amount of Cell-Cell Contact Demonstrates Biphasic Proliferative Regulation through Rhoa and the Actin Cytoskeleton. *Exp. Cell Res.* **2008**, *314*, 2846–2854.
(10) Brandley, B. K.; Schnaar, R. L. Cell-Surface Carbohydrates in Cell Recognition and Response. *J. Leukocyte Biol.* **1986**, *40*, 97–111.
(11) Schwarz, J.; Sixt, M. Quantitative Analysis of Dendritic Cell Haptotaxis. *Methods Enzymol.* **2016**, *570*, 567–581.
(12) Wu, J.; Mao, Z.; Tan, H.; Han, L.; Ren, T.; Gao, C. Gradient Biomaterials and Their Influences on Cell Migration. *Interface Focus* **2012**, *2*, 337–355.
(13) Azioune, A.; Storch, M.; Bornens, M.; Théry, M.; Piel, M. Simple and Rapid Process for Single Cell Micro-Patterning. *Lab Chip* **2009**, *9*, 1640–1642.
(14) Whitesides, G. M.; Ostuni, E.; Takayama, S.; Jiang, X.; Ingber, D. E. Soft Lithography in Biology and Biochemistry. *Annu. Rev. Biomed. Eng.* **2001**, *3*, 335–373.
(15) Gegenfurtner, F. A.; Jahn, B.; Wagner, H.; Ziegenhain, C.; Enard, W.; Geistlinger, L.; Rädler, J. O.; Vollmar, A. M.; Zahler, S. Micropatterning as a Tool to Identify Regulatory Triggers and Kinetics of Actin-Mediated Endothelial Mechanosensing. *J. Cell Sci.* **2018**, *131*, No. jcs212886.
(16) Mohammed, D.; Charras, G.; Vercruysse, E.; Versaevel, M.; Lantoine, J.; Alaimo, L.; Bruyère, C.; Luciano, M.; Glinel, K.; Delhaye, G.; Théodoly, O.; Gabriele, S. Substrate Area Confinement Is a Key Determinant of Cell Velocity in Collective Migration. *Nat. Phys.* **2019**, *15*, 858–866.
(17) Chen, T.; Callan-Jones, A.; Fedorov, E.; Ravasio, A.; Brugues, A.; Ong, H. T.; Toyama, Y.; Low, B. C.; Trepat, X.; Shemesh, T.; Voituriez, R.; Ladoux, B. Large-Scale Curvature Sensing by Directional Actin Flow Drives Cellular Migration Mode Switching. *Nat. Phys.* **2019**, *15*, 393–402.
(18) Holden, M. A.; Cremer, P. S. Light Activated Patterning of Dye-Labeled Molecules on Surfaces. *J. Am. Chem. Soc.* **2003**, *125*, 8074–8075.
(19) Shirai, K.; Renberg, B.; Sato, K.; Mawatari, K.; Konno, T.; Ishihara, K.; Kitamori, T. Graft Linker Immobilization for Spatial Control of Protein Immobilization inside Fused Microchips. *Electrophoresis* **2009**, *30*, 4251–4255.
(20) Strale, P. O.; Azioune, A.; Bugnicourt, G.; Lecomte, Y.; Chahid, M.; Studer, V. Multiprotein Printing by Light-Induced Molecular Adsorption. *Adv. Mater.* **2016**, *28*, 2024–2029.
(21) Martin, T. A.; Herman, C. T.; Limpoco, F. T.; Michael, M. C.; Potts, G. K.; Bailey, R. C. Quantitative Photochemical Immobilization of Biomolecules on Planar and Corrugated Substrates: A Versatile Strategy for Creating Functional Biointerfaces. *ACS Appl. Mater. Interfaces* **2011**, *3*, 3762–3771.
(22) Larsen, E. K. U.; Mikkelsen, M. B. L.; Larsen, N. B. Protein and Cell Patterning in Closed Polymer Channels by Photoimmobilizing Proteins on Photografted Poly(Ethylene Glycol) Diacrylate. *Biomicrofluidics* **2014**, *8*, No. 064127.
(23) Preston, G. W.; Wilson, A. J. Photo-Induced Covalent Cross-Linking for the Analysis of Biomolecular Interactions. *Chem. Soc. Rev.* **2013**, *42*, 3289–3301.
(24) Yamamoto, N.; Bernardi, F.; Bottoni, A.; Olivucci, M.; Robb, M. A.; Wilsey, S. Mechanism of Carbene Formation from the Excited States of Diazirine and Diazomethane: An MC-SCF Study. *J. Am. Chem. Soc.* **1994**, *116*, 2064–2074.
(25) Gomes, A. F.; Gozzo, F. C. Chemical Cross-Linking with a Diazirine Photoactivatable Cross-Linker Investigated by MALDI- and ESI-MS/MS. *J. Mass Spectrom.* **2010**, *45*, 892–899.
(26) Rostovtsev, V. V.; Green, L. G.; Fokin, V. V.; Sharpless, K. B. A Stepwise Huisgen Cycloaddition Process: Copper(I)-Catalyzed Regioselective "Ligation" of Azides and Terminal Alkynes. *Angew. Chem., Int. Ed.* **2002**, *41*, 2596–2599.
(27) Jewett, J. C.; Bertozzi, C. R. Cu-Free Click Cycloaddition Reactions in Chemical Biology. *Chem. Soc. Rev.* **2010**, *39*, 1272–1279.
(28) Carrico, I. S.; Maskarinec, S. A.; Heilshorn, S. C.; Mock, M. L.; Liu, J. C.; Nowatzki, P. J.; Franck, C.; Ravichandran, G.; Tirrell, D. A. Lithographic Patterning of Photoreactive Cell-Adhesive Proteins. *J. Am. Chem. Soc.* **2007**, *129*, 4874–4875.
(29) Wirkner, M.; Weis, S.; San Miguel, V.; Alvarez, M.; Gropeanu, R. A.; Salierno, M.; Sartoris, A.; Unger, R. E.; Kirkpatrick, C. J.; Del Campo, A. Photoactivatable Caged Cyclic RGD Peptide for Triggering Integrin Binding and Cell Adhesion to Surfaces. *Chembiochem* **2011**, *12*, 2623–2629.

(30) Rosch, J. C.; Hollmann, E. K.; Lippmann, E. S. In Vitro Selection Technologies to Enhance Biomaterial Functionality. *Exp. Biol. Med.* **2016**, *241*, 962−971.
(31) Bellis, S. L. Advantages of RGD Peptides for Directing Cell Association with Biomaterials. *Biomaterials* **2011**, *32*, 4205−4210.
(32) Hersel, U.; Dahmen, C.; Kessler, H. RGD Modified Polymers: Biomaterials for Stimulated Cell Adhesion and Beyond. *Biomaterials* **2003**, *24*, 4385−4415.
(33) Takada, Y.; Ye, X.; Simon, S. The Integrins. *Genome Biol.* **2007**, *8*, No. 215.
(34) Ruoslahti, E. Fibronectin and its Receptors. *Annu. Rev. Biochem.* **1988**, *57*, 375−413.
(35) Kapp, T. G.; Rechenmacher, F.; Neubauer, S.; Maltsev, O. V.; Cavalcanti-Adam, E. A.; Zarka, R.; Reuning, U.; Notni, J.; Wester, H.-J.; Mas-Moruno, C.; Spatz, J.; Geiger, B.; Kessler, H. A Comprehensive Evaluation of the Activity and Selectivity Profile of Ligands for RGD-Binding Integrins. *Sci. Rep.* **2017**, *7*, No. 39805.
(36) Knight, C. G.; Morton, L. F.; Peachey, A. R.; Tuckwell, D. S.; Farndale, R. W.; Barnes, M. J. The Collagen-binding A-domains of Integrins $\alpha1\beta1$ and $\alpha2\beta1$ Recognize the Same Specific Amino Acid Sequence, GFOGER, in Native (Triple-Helical) Collagens. *J. Biol. Chem.* **2000**, *275*, 35−40.
(37) Boateng, S. Y.; Lateef, S. S.; Mosley, W.; Hartman, T. J.; Hanley, L.; Russell, B. RGD and YIGSR Synthetic Peptides Facilitate Cellular Adhesion Identical to that of Laminin and Fibronectin but Alter the Physiology of Neonatal Cardiac Myocytes. *Am. J. Physiol.: Cell Physiol.* **2005**, *288*, C30−C38.
(38) Ruoslahti, E. Rgd and Other Recognition Sequences for Integrins. *Annu. Rev. Cell Dev. Biol.* **1996**, *12*, 697−715.
(39) Mrksich, M.; Whitesides, G. M. Using Self-Assembled Monolayers to Understand the Interactions of Man-Made Surfaces with Proteins and Cells. *Annu. Rev. Biophys. Biomol. Struct.* **1996**, *25*, 55−78.
(40) Lussi, J. W.; Falconnet, D.; Hubbell, J. A.; Textor, M.; Csucs, G. Pattern Stability under Cell Culture Conditions—A Comparative Study of Patterning Methods Based on PLL-G-Peg Background Passivation. *Biomaterials* **2006**, *27*, 2534−2541.
(41) Nelson, C. M.; Raghavan, S.; Tan, J. L.; Chen, C. S. Degradation of Micropatterned Surfaces by Cell-Dependent and -Independent Processes. *Langmuir* **2003**, *19*, 1493−1499.
(42) Sugawara, T.; Matsuda, T. Photochemical Surface Derivatization of a Peptide Containing Arg−Gly−Asp (Rgd). *J. Biomed. Mater. Res.* **1995**, *29*, 1047−1052.
(43) Doyle, A. D. *Generation of Micropatterned Substrates Using Micro Photopatterning*; John Wiley & Sons, Inc., 2001.
(44) Doyle, A. D.; Wang, F. W.; Matsumoto, K.; Yamada, K. M. One-Dimensional Topography Underlies Three-Dimensional Fibrillar Cell Migration. *J. Cell Biol.* **2009**, *184*, 481−490.
(45) Weber, M.; Sixt, M. Live Cell Imaging of Chemotactic Dendritic Cell Migration in Explanted Mouse Ear Preparations. *Methods Mol. Biol.* **2013**, *1013*, 215−226.
(46) Middleton, J.; Neil, S.; Wintle, J.; Clark-Lewis, I.; Moore, H.; Lam, C.; Auer, M.; Hub, E.; Rot, A. Transcytosis and Surface Presentation of IL-8 by Venular Endothelial Cells. *Cell* **1997**, *91*, 385−395.
(47) Stirman, J. N.; Crane, M. M.; Husson, S. J.; Gottschalk, A.; Lu, H. A Multispectral Optical Illumination System with Precise Spatiotemporal Control for the Manipulation of Optogenetic Reagents. *Nat. Protoc.* **2012**, *7*, 207−220.
(48) Wu, Y. I.; Frey, D.; Lungu, O. I.; Jaehrig, A.; Schlichting, I.; Kuhlman, B.; Hahn, K. M. A Genetically Encoded Photoactivatable Rac Controls the Motility of Living Cells. *Nature* **2009**, *461*, 104−108.
(49) Friedrich, J.; Seidel, C.; Ebner, R.; Kunz-Schughart, L. A. Spheroid-Based Drug Screen: Considerations and Practical Approach. *Nat. Protoc.* **2009**, *4*, 309−324.
(50) Moffat, J. G.; Rudolph, J.; Bailey, D. Phenotypic Screening in Cancer Drug Discovery—Past, Present and Future. *Nat. Rev. Drug Discov.* **2014**, *13*, 588−602.
(51) Schreiber, C.; Segerer, F. J.; Wagner, E.; Roidl, A.; Rädler, J. O. Ring-Shaped Microlanes and Chemical Barriers as a Platform for Probing Single-Cell Migration. *Sci. Rep.* **2016**, *6*, No. 26858.
(52) Murschhauser, A.; Röttgermann, P. J. F.; Woschée, D.; Ober, M. F.; Yan, Y.; Dawson, K. A.; Rädler, J. O. A High-Throughput Microscopy Method for Single-Cell Analysis of Event-Time Correlations in Nanoparticle-Induced Cell Death. *Commun. Biol.* **2019**, *2*, No. 35.
(53) Jang, K.; Xu, Y.; Tanaka, Y.; Sato, K.; Mawatari, K.; Konno, T.; Ishihara, K.; Kitamori, T. Single-Cell Attachment and Culture Method Using a Photochemical Reaction in a Closed Microfluidic System. *Biomicrofluidics* **2010**, *4*, No. 032208.
(54) Siekmann, A. F.; Affolter, M.; Belting, H. G. The Tip Cell Concept 10 Years After: New Players Tune in for a Common Theme. *Exp. Cell Res.* **2013**, *319*, 1255−1263.
(55) Kurz, H.; Gartner, T.; Eggli, P. S.; Christ, B. First Blood Vessels in the Avian Neural Tube Are Formed by a Combination of Dorsal Angioblast Immigration and Ventral Sprouting of Endothelial Cells. *Dev. Biol.* **1996**, *173*, 133−147.
(56) Mack, J. J.; Iruela-Arispe, M. L. Notch Regulation of the Endothelial Cell Phenotype. *Curr. Opin. Hematol.* **2018**, *25*, 212−218.
(57) Schuster, S. L.; Segerer, F. J.; Gegenfurtner, F. A.; Kick, K.; Schreiber, C.; Albert, M.; Vollmar, A. M.; Radler, J. O.; Zahler, S. Contractility as a Global Regulator of Cellular Morphology, Velocity, and Directionality in Low-Adhesive Fibrillary Micro-Environments. *Biomaterials* **2016**, *102*, 137−147.
(58) Behrndt, M.; Salbreux, G.; Campinho, P.; Hauschild, R.; Oswald, F.; Roensch, J.; Grill, S. W.; Heisenberg, C. P. Forces Driving Epithelial Spreading in Zebrafish Gastrulation. *Science* **2012**, *338*, 257−260.
(59) Stirman, J. N.; Crane, M. M.; Husson, S. J.; Wabnig, S.; Schultheis, C.; Gottschalk, A.; Lu, H. Real-Time Multimodal Optical Control of Neurons and Muscles in Freely Behaving Caenorhabditis elegans. *Nat. Methods* **2011**, *8*, 153−158.
(60) Edelstein, A.; Amodaj, N.; Hoover, K.; Vale, R.; Stuurman, N. Computer Control of Microscopes Using μmanager. *Curr. Protoc. Mol. Biol.* **2010**, *92*, 14.20.1−14.20.17.
(61) Schneider, C. A.; Rasband, W. S.; Eliceiri, K. W. NIH Image to Imagej: 25 Years of Image Analysis. *Nat. Methods* **2012**, *9*, 671−675.
(62) Schindelin, J.; Arganda-Carreras, I.; Frise, E.; Kaynig, V.; Longair, M.; Pietzsch, T.; Preibisch, S.; Rueden, C.; Saalfeld, S.; Schmid, B.; Tinevez, J. Y.; White, D. J.; Hartenstein, V.; Eliceiri, K.; Tomancak, P.; Cardona, A. Fiji: An Open-Source Platform for Biological-Image Analysis. *Nat. Methods* **2012**, *9*, 676−682.
(63) Fabrice, P. Cordelières Manuel Tracking Image J. https://imagej.nih.gov/ij/plugins/manual-tracking.html (accessed April 21, 2021).
(64) Sommer, C.; Straehle, C.; Köthe, U.; Hamprecht, F. A. Ilastik: Interactive Learning and Segmentation Toolkit. In *2011 IEEE International Symposium on Biomedical Imaging: From Nano to Macro*, **2011**; pp 230−233.

https://doi.org/10.1021/acsami.1c09850
ACS Appl. Mater. Interfaces 2021, 13, 35545−35560